size and size distribution even after overnight incubation in 10% FBS-containing media (Figure 3C), indicating the high stability of these nanoarchitectures in the biological media. These results clearly demonstrate that the uPIC-AuNPs were successfully constructed in a size-regulated and monodispersed manner.

Next, the number of uPICs (or siRNAs) loaded in the uPIC-AuNPs was determined using a fluorescently labeled siRNA. The uPIC-AuNPs prepared with Alexa647-labeled siRNA (Alexa-siRNA) were treated with an excess amount of mercaptoethanol (12 mM) to induce a thiol exchange reaction on the AuNP surface.[19] The amount of released uPIC was quantified from its fluorescence intensity in the supernatant according to the standard curve (Figure S3 (SI)), and normalized by the amount of AuNP in solution. The number of loaded uPICs was calculated to be *ca.* 20 per AuNP. This value is slightly smaller than that for previous siRNA-loaded AuNP systems, where thiolated siRNAs were directly attached to AuNPs and the number of loaded siRNA amounted to *ca.* 30 per AuNP.[26] The difference between these two formulations could be explained by their different spacer length between thiol and the charged segment. The thiolated siRNA had a longer spacer than the present PEG-PLL-SH polymer, alleviating the steric repulsive effects on the AuNP surface.

With regard to the nanoconstruction of uPIC-AuNPs, it was verified whether the preformation of uPICs and the thiol moiety in PEG-PLL-SH were indispensable for successful preparation of the uPIC-AuNPs. When PEG-PLL-SH polymers were directly mixed with AuNPs prior to PIC formation (or in the absence of siRNA), visible flocculates were formed as indicated by the red-shift in their UV–vis absorbance spectrum (Figure 3A),[18] probably due to consecutive electrostatic binding between negatively charged citrate-stabilized AuNPs and oppositely charged PLL segments. On the other hand, the mixing between AuNPs and uPICs prepared with nonthiolated PEG-PLL led to the formation of considerably larger nanoparticles (DLS peak top: ~120 nm) with a broader size distribution (Figure 3C) and a slightly broader absorbance spectrum (Figure 3A) compared to the uPIC-AuNPs. This result indicates that a large number of AuNPs aggregated into larger particles under the physiological salt condition as a result of low colloidal stability through ineffective surface PEGylation in the absence of thiol-gold coordinate bonding. Note that bare AuNPs immediately aggregated to form visible flocculates by salting-out effect under the same condition (data not shown). Thus, the successful preparation of uPIC-AuNPs may stem from (i) the charge-neutralization of cationic PLL segment with siRNA, which reduces the electrostatic adsorptions between PLL chains and AuNPs, and (ii) the effective conjugation of uPICs (or PEG chains) onto AuNPs through thiol-gold coordinate bonding, which enhances colloidal stability.

The reversible stability of uPIC-AuNPs was verified by mimicking cytoplasmic reductive conditions as well as the extracellular conditions. The nanoarchitectures were incubated in a heparin solution with or without 10 mM GSH, which corresponds to the cytoplasmic concentration. In this stability assay, heparin was used as a representative of glycocalyx that is a major component of extracellular matrices and is abundant in the renal basement membrane. Glycocalyx is considered as a major obstacle for PIC-based siRNA delivery because PICs might be disrupted through electrostatic interactions with the negatively charged matrices.[27] In the absence of heparin and GSH, almost no bands derived from siRNA were observed for both uPICs and uPIC-AuNPs (Figure 4A), confirming the polyionic complexation of siRNA as indicated by the FCS result (Figure 2A). It should be noted that the staining of siRNA with SYBR Green II was significantly impaired when siRNA forms PICs with PEG-PLL, leading to almost no fluorescence signal from the siRNAs loaded by uPICs as well as uPIC-AuNPs. The heparin treatment induced a concentration-dependent siRNA release from uPICs and uPIC-AuNP by counter polyanion exchange. However, this release required more heparin in the case of uPIC-AuNPs compared to uPICs. In particular, while the released siRNA was clearly observed upon treatment of uPICs with 1 $\mu$g/mL of heparin, almost no band was detected for uPIC-AuNPs under the same conditions. These results indicate that uPICs conjugated onto the AuNP were more stable than free uPICs. This enhanced PIC stability may be attributed to the PEG outer layer surrounding uPIC-AuNP.

In contrast, the GSH-treated uPIC-AuNPs showed a band of released siRNA with smaller amount of heparin, compared to those in the absence of GSH, demonstrating the GSH-responsive siRNA release from uPIC-AuNPs. The underlying mechanism for this GSH-responsive release can be explained as follows. GSH (or its cystein thiol) can detach uPICs from AuNP through the thiol–thiol exchange reaction. The detached uPICs should become more sensitive for counter polyanion exchange with heparin as indicated by Figure 4A (uPIC + Heparin lanes *vs* uPIC-AuNP + Heparin lanes), resulting in the facilitated siRNA release. This can be explained by the fact that the cysteine thiol in GSH can competitively interact with coordinate bonds between uPICs and AuNP, forming alternative coordinate bonds with AuNPs (or uPICs) that promote the detachment of uPICs from uPIC-AuNPs. In this regard, it is worth mentioning that the GSH-treated uPIC-AuNPs also released siRNA in the absence of heparin. GSH alone did not release siRNA from uPICs even at 50 mM (Figure 4B), suggesting that the coexistence of GSH and AuNPs should be crucial for the siRNA release. We assumed that GSH-conjugated AuNPs (GSH-AuNPs), which should be generated by incubation of uPIC-AuNPs with GSH, might elicit siRNA release from

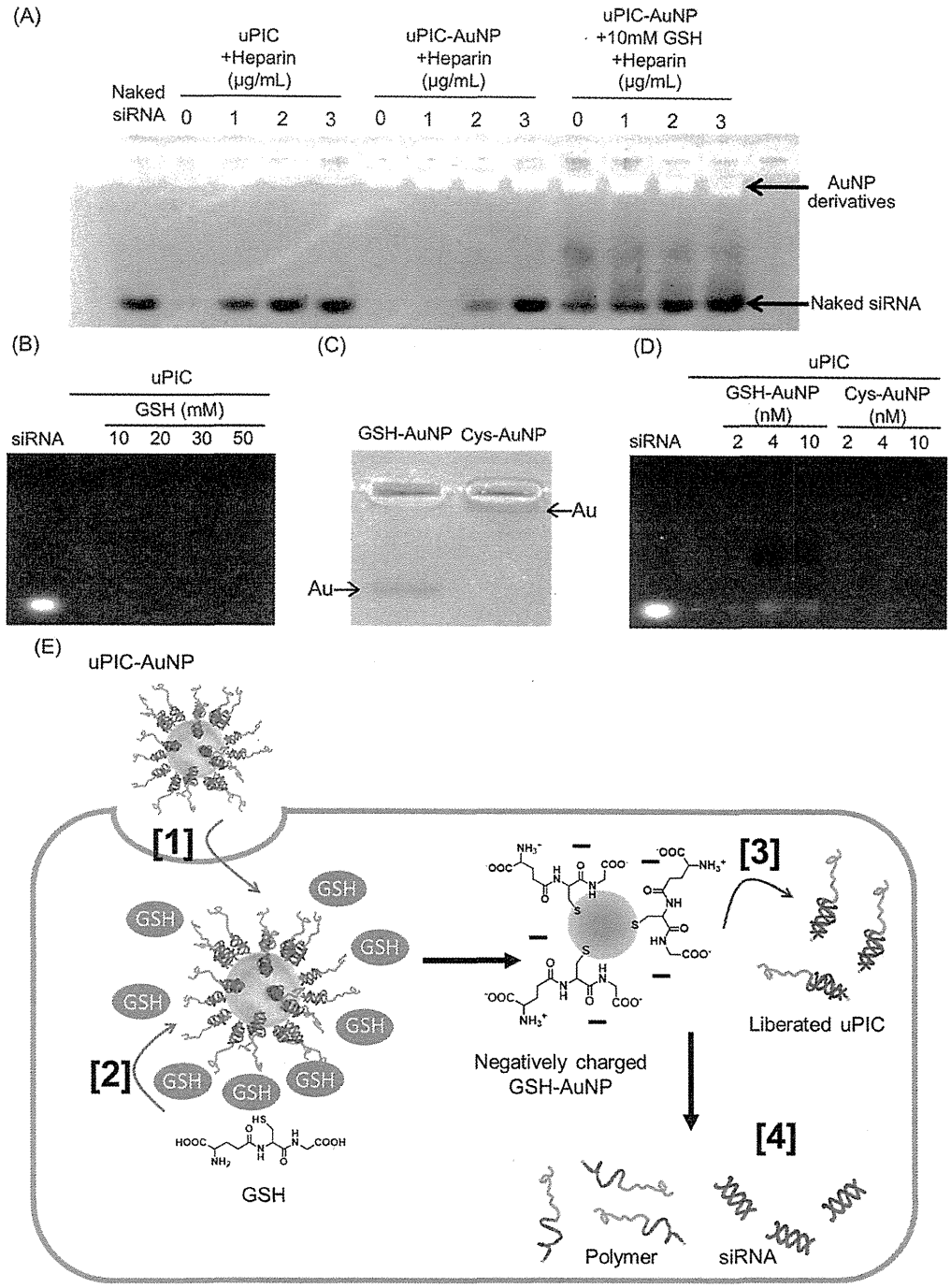


**Figure 4. (A) Stability assay of uPICs and uPIC-AuNPs (400 nM siRNA) incubated with heparin (0, 1, 2, and 3 μg/mL) and GSH (0 and 10 mM). At 10 min after incubation, the solutions were loaded onto 1% agarose gel (1 × Tris/Borate/EDTA (TBE) buffer), subjected to a voltage of 100 V for 15 min, and stained with SYBR Green II. (B) Gel electrophoresis of uPICs solutions in the presence of various GSH concentrations. (C) Gel electrophoresis of AuNPs solutions treated with GSH or cysteine. Arrows indicate the AuNP positions. (D) Gel electrophoresis of uPICs solutions in the presence of AuNPs pretreated with GSH (GSH-AuNP) or with cysteine (Cys-AuNP). (E) Schematic illustration of the proposed mechanism for intracellular siRNA release from uPIC-AuNPs in the presence of GSH.**

uPICs; the GSH-AuNPs that have negative surface charges derived from one excess of carboxyl group in GSH can bind to oppositely charged PEG-PLL in uPICs, directed toward siRNA release. To verify this assumption, an additional release assay was performed using GSH-AuNPs prepared as a negatively charged nanoparticle and cysteine-conjugated AuNPs (Cys-AuNPs) which were prepared as a control nanoparticle

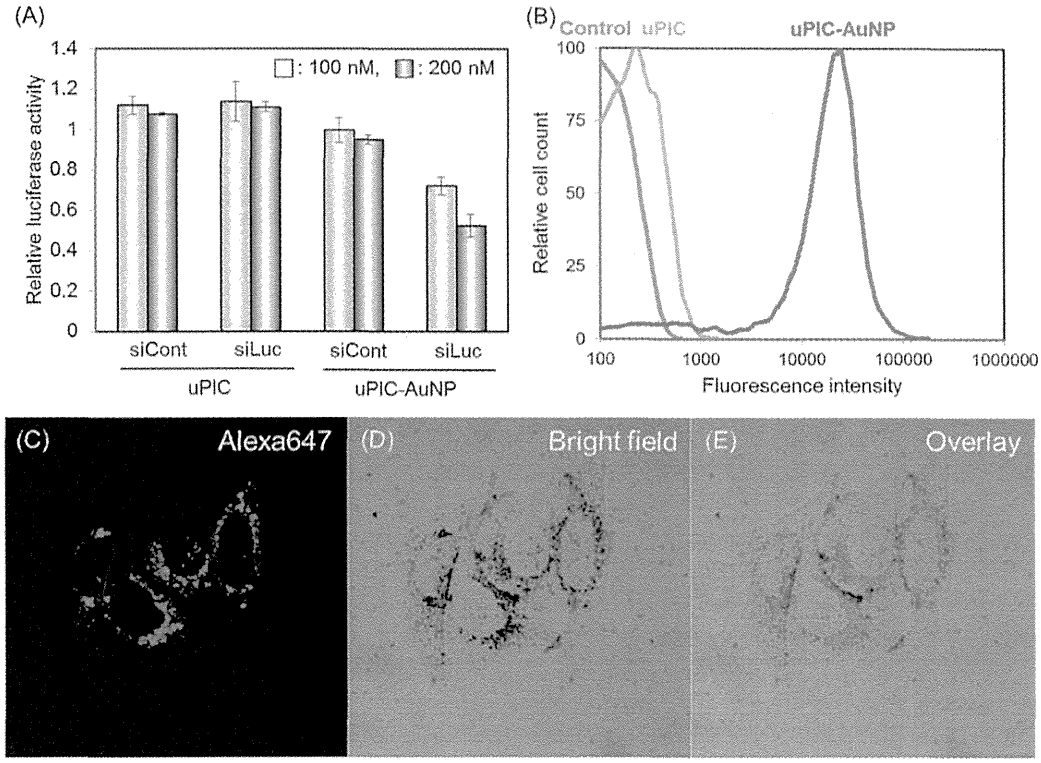


**Figure 5. (A) Gene silencing efficiency of uPICs and uPIC-AuNPs loaded with siLuc or siCont at 100 and 200 nM siRNA in cultured HeLa-Luc cells after 48 h incubation. Results are expressed as mean and standard deviation ($n$ = 4). (B) Flow cytometry analysis of siRNA cellular uptake efficiency in cultured HeLa-Luc cells incubated for 24 h with uPIC-AuNPs or uPICs at 200 nM Alexa-siRNA. (C–E) CLSM images of HeLa-Luc cells treated with uPIC-AuNPs at 200 nM Alexa-siRNA for 24 h.**

modified with a neutral amino acid. The significant negative charges of GSH-AuNPs were confirmed by the agarose gel electrophoresis (Figure 4C), where GSH-AuNPs were clearly shifted to the positive electrode, compared to Cys-AuNPs. As expected, GSH-AuNPs permitted siRNA release from uPICs in a concentration-dependent manner (Figure 4D). In contrast, much lower amounts of released siRNA were detected using Cys-AuNPs (Figure 4D). These results are consistent with the above assumption that the negative charges derived from GSH conjugated on AuNPs should be crucial for the effective release of siRNA from uPICs. Altogether, it is strongly suggested that the uPIC-AuNPs internalized by cells should accelerate siRNA release in response to abundant cytoplasmic GSH, as illustrated in Figure 4E.

The stability of uPIC-AuNPs was further compared with a control conjugate without PEG-PLL (siRNA-AuNP), which was prepared by mixing thiolated siRNAs with AuNPs. In this stability assay, each conjugate prepared with Cy5-siRNA was incubated in 10 mM Hepes buffer (pH 7.2) containing 150 mM NaCl and 10% FBS. The fluorescence intensity derived from Cy5 was sequentially monitored using a plate reader, then normalized to that of free Cy5-siRNA (Figure S4 (SI)). The increase in the fluorescence intensity, presumably due to the dequenching effect of Cy5, was smaller in uPIC-AuNPs compared to siRNA-AuNPs, indicating that the uPIC-AuNPs more effectively suppressed disintegration of the conjugate structure (or degradation of siRNA) in the serum-containing medium. This result demonstrates an advantage of the conjugate formulation using PEG-PLL.

**Cellular Delivery of siRNA with uPIC-AuNPs.** Cellular delivery of siRNA by uPIC-AuNPs was first investigated by a luciferase assay, in which the gene silencing of uPIC-AuNPs was evaluated from the luciferase activity (or luminescence intensity) in cultured cervical cancer cells stably expressing luciferase (HeLa-Luc). Nanoarchitectures bearing luciferase siRNA (siLuc) or control siRNA (siCont) were incubated with HeLa-Luc cells for 48 h prior to the measurement of luminescence intensity. The uPIC-AuNPs carrying siLuc significantly reduced the luciferase activity, *i.e.*, ~25 and ~40% at 100 and 200 nM siRNA, respectively, whereas siCont-loaded controls showed no decrease in the luciferase activity (Figure 5A), demonstrating the sequence-specific gene silencing effect of uPIC-AuNPs. In sharp contrast, siLuc-loaded uPICs without AuNPs induced no gene silencing effect at both siRNA concentrations. These results indicate that the AuNPs templates were indispensable in enhancing the gene silencing effect

of uPIC-AuNPs. The gene silencing efficiency obtained by uPIC-AuNPs was apparently similar and lower compared to previously reported siRNA-conjugated AuNPs[26] and their complexes with cationic poly(β-amino ester)s,[28] respectively. The lower efficiency may be due to the PEG outer layer on uPIC-AuNP surface, which can compromise the adsorptive endocytosis of nanoparticles through the steric repulsive effect,[5] leading to less cellular uptake of siRNA compared to the positively charged nanoparticle carrier. Cell viability was further examined in cultured HeLa-Luc cells under the similar condition to the luciferase assay (Figure S5 (SI)). Neither uPIC-AuNPs nor uPICs affected the cell viability until 400 nM siRNA. Thus, negligible cytotoxic effect was confirmed for these formulations.

In order to elucidate which step in the cellular delivery of siRNA generated the dramatic improvement in the gene silencing effect of uPIC-AuNPs, we further addressed cellular uptake and intracellular trafficking studies using Alexa-siRNA. The cellular uptake efficiency of Alexa-siRNA was determined by flow cytometric analyses for the HeLa-Luc cells incubated with uPIC-AuNPs or uPICs at 200 nM Alexa-siRNA for 24 h (Figure 5B). Cells treated with uPIC-AuNPs exhibited 70-fold higher mean fluorescence intensity than those with uPICs without AuNPs, indicating a significantly enhanced cellular uptake of siRNA upon conjugation of uPIC to AuNPs. It should be further noted that the enhanced cellular uptake of uPIC-AuNPs was clearly observed even after treating the cells with a heparin/DTT solution after 6 and 24 h incubation (Figure S6 (SI)), suggesting that the Alexa-siRNA payloads should be within the cells but not bound to the cellular surface. This result matches the greater gene silencing effect of uPIC-AuNPs (Figure 5A). The higher efficiency of the cellular uptake of uPIC-AuNPs may be attributed to their higher stability against counter polyion exchange with negatively charged glycosaminoglycans, compared to uPICs (Figure 4A). uPIC-AuNPs should be more stable on the cell surface coated with anionic glycocalyx,[29] facilitating the cellular uptake of siRNA through charge-neutralization and reduced electrostatic repulsion between siRNA and the cell surface. The detailed mechanism for the cellular uptake of uPIC-AuNPs remains to be further investigated. The intracellular trafficking of uPIC-AuNPs was observed by a confocal laser scanning microscope (CLSM) (Figure 5C–E). While cells treated with uPICs exhibited almost no fluorescence (Figure S7 (SI)), the fluorescent signal of Alexa-siRNA was clearly observed in cells treated with uPIC-AuNPs (Figure 5C), consistent with flow cytometric results (Figure 5B). The bright field image depicts that numerous AuNPs were concurrently internalized by the cells and mainly distributed in the perinuclear region (Figure 5D). Based on the overlay image (Figure 5E), the correlation between intracellular Alexa-siRNA and AuNPs was then calculated to be nearly 1 by Mander's correlation coefficient. This high level of the correlation strongly suggests that siRNA molecules (or uPICs) are internalized together with AuNPs and subsequently delivered to the perinuclear regions, such as the late endosome or lysosome, by microtubule tracking.[30] Accordingly, siRNA translocation from the endosome or lysosome to the cytoplasm will be one of the critical steps for improving the gene silencing efficiency in a future study.

**Systemic Delivery of siRNA to a Subcutaneous Tumor Model using uPIC-AuNPs.** As demonstrated in many previous studies, sub-100 nm-sized nanoparticles featuring longevity in circulation can efficiently accumulate in solid tumors through the leaky tumor vasculature and immature lymphatic drainage *via* EPR effect.[11,12] The MW of uPICs was determined to be 22 000 Da by the AUC method, thereby they are expected to be eliminated by renal filtration.[31] Indeed, it was demonstrated that 90% of uPICs prepared with Alexa-siRNA were eliminated from the bloodstream in 10 min after intravenous injection (Figure S8 (SI)), when the fluorescence intensity from the vein of murine earlobe was time-dependently monitored by an intravital real-time confocal laser scanning microscope.[32,33] Thus, we conjugated uPICs onto AuNPs (20 nm in diameter) to regulate the carrier size for evading such rapid clearance, directed toward longer blood circulation. The uPIC-AuNPs (or bare AuNPs as a control) were injected intravenously into mice and blood samples were collected after a designated time. The concentration of AuNP in plasma was determined by ion coupled plasma-mass spectrometer (ICP-MS) and normalized to the initial dose. Note that the blood circulation time of uPIC-AuNPs was estimated by ICP-MS instead of confocal laser scanning microscope because the fluorescence intensity of Alexa-siRNA was considerably quenched on the AuNP surface. The time for 90% elimination of uPIC-AuNPs (*ca.* 180 min) was three times longer than that for bare AuNPs (*ca.* 60 min) (Figure 6A) and 1 order of magnitude longer than that for uPICs (*ca.* 10 min). The longer blood circulation time in uPIC-AuNP should be attributed to its uniformly controlled size at *ca.* 40 nm, circumventing renal filtration. This result also indicates that the uPICs conjugated on the AuNP significantly improved the blood circulation longevity of AuNPs, presumably because the PEG outer layer reduced nonspecific interactions with blood components.[5,34]

Next, the accumulation of systemically administered uPIC-AuNPs in subcutaneous HeLa-Luc tumors was evaluated based on the fluorescence intensity of excised tumors using an *in vivo* imaging system (IVIS) instrument and compared with several controls, such as naked siRNA, uPICs, and the mixture of AuNPs and uPICs without thiol (Figure 6B). The fluorescence intensities of Alexa-siRNA delivered by uPICs or the

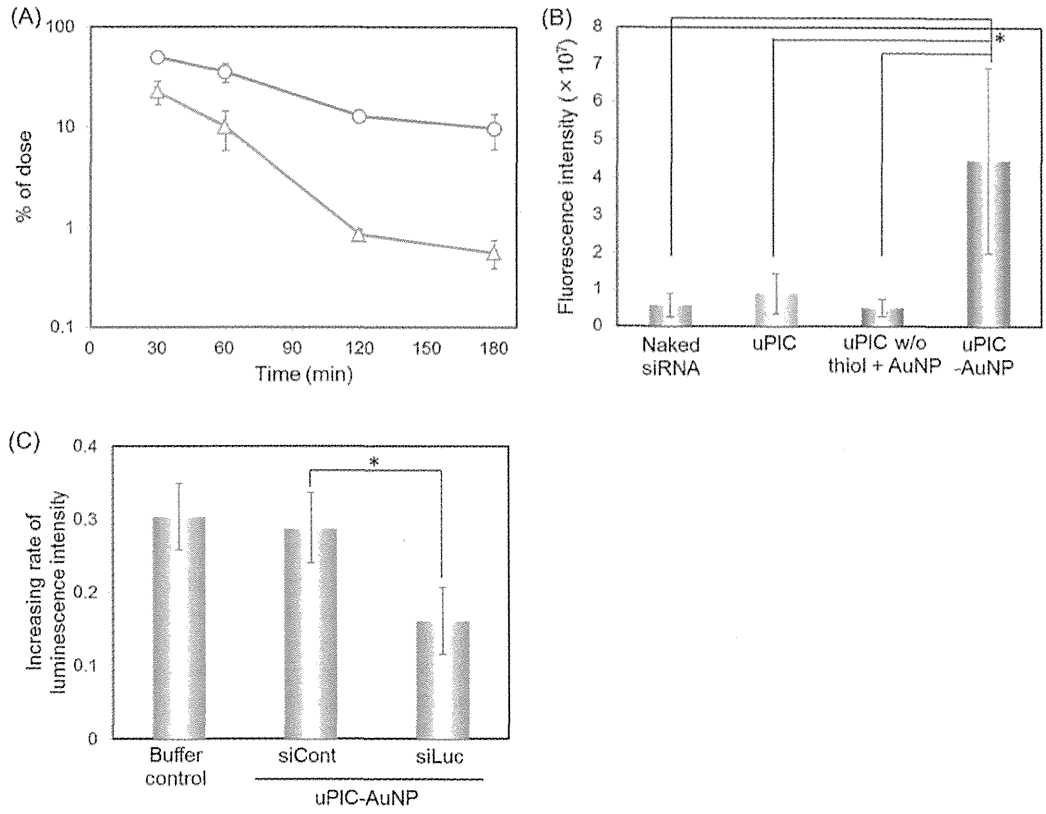


**Figure 6. (A) Blood circulation property of uPIC-AuNPs (open circle) and bare AuNPs as a control (open triangle) determined by ICP-MS. Results are expressed as mean and standard deviation ($n = 3-4$). (B) Subcutaneous HeLa-Luc tumor accumulation of Alexa-siRNA delivered by each formulation at 4 h after intravenous injection (4.8 $\mu$g siRNA/mouse), determined by IVIS. Results are expressed as mean and standard deviation ($n = 4$, *: $P < 0.01$). (C) Increasing rate of luminescence intensity ($IR_{LI}$) from subcutaneous HeLa-Luc tumors after treatment with siLuc- or siCont-loaded uPIC-AuNPs (5.8 $\mu$g siRNA/mouse/shot) or a Hepes buffer control. The $IR_{LI}$ values were calculated as an indicator of luciferase gene silencing activity, as described in the Materials and Methods. Results are expressed as mean and standard error of the mean ($n = 4$, *$P < 0.05$).**

mixture of AuNP/uPICs without thiol were similar to that of naked Alexa-siRNA. In contrast, a significantly higher fluorescence intensity was observed for uPIC-AuNPs ($p < 0.01$ for the other samples), indicating the enhanced tumor accumulation of uPIC-AuNPs. This fluorescence intensity in the tumor was converted to $14 \pm 4$ in terms of % dose/g of tumor using a standard curve. Note that the fluorescence intensity of uPIC-AuNPs was likely to be underestimated compared to free uPICs because of the quenching effect of AuNPs: *ca.* 65% of the fluorescence signal was quenched in the uPIC-AuNPs. Apparently, this result is correlated with the blood circulation property of delivery carriers, as the efficient tumor accumulation was achieved by the long-circulating uPIC-AuNPs. Furthermore, the comparison between uPIC-AuNPs and the mixture of AuNP/uPICs without thiol reveals the key role of the strong binding between uPICs and AuNPs for the enhanced tumor accumulation of siRNA. Weakly bound uPICs on AuNPs might be readily detached from the nanotemplate in the circulation, presumably leading to the renal filtration, similar to uPICs without AuNPs and naked siRNA.

Finally, the gene silencing efficiency of systemically administered uPIC-AuNPs was investigated in subcutaneous HeLa-Luc tumors by the luciferase assay. The luminescence intensity emitted from HeLa-Luc tumors was measured using an IVIS instrument after intraperitoneal injection of a luciferin substrate. An increasing rate of luminescence intensity was significantly reduced to approximately 50% in the tumors treated with siLuc-containing uPIC-AuNPs, compared to a buffer-treated control and siCont-containing uPIC-AuNPs (Figure 6C). Thus, the uPIC-AuNPs were demonstrated to successfully induce the sequence-specific gene silencing in the tumor tissue through systemic administration, probably due to the efficient tumor accumulation associated with its longevity in the blood. It should be noted that severe cytokine induction was not observed after systemic administration of uPIC-AuNPs at the similar dose (Figure S10 (SI)). Interestingly, a slight increase in the TNF-α level observed for bare AuNPs at 6 h after injection was apparently reduced in uPIC-AuNPs, possibly due to the biologically inert PEGylated surface of uPIC-AuNPs.

Recent studies, including ours, revealed that precise size controlling below 100 nm had a great impact on the nanoparticle accumulation and permeation in a variety of tumor models. Specifically, sub-50 nm-sized nanoparticles achieved considerably higher accumulation efficiency in thick fibrotic pancreatic tumor tissues compared to 100 nm-sized controls.[13] The methodology developed in this study can build size-tunable nanoarchitectures featuring monodispersed uPIC building blocks and size-preset AuNP nanotemplates. Consequently, the constructed uPIC-AuNP nanoarchitectures enabled the efficient tumor accumulation of siRNA and significant *in vivo* gene silencing effect in the tumor, demonstrating their potential for siRNA-based cancer therapies.

## CONCLUSIONS

In the present study, the size-tunable and reversibly stabilized nanoarchitecture was constructed with a monodispersed building block of uPICs and a size-preset nanotemplate of AuNPs for systemic siRNA delivery to solid tumors. The monodispersed uPICs were prepared with a single charged pair of siRNA and PEG-PLL-SH with the $DP_{PLL}$ = ~40 based on the charge-matched polyionic complexation. Then, the uPICs were conjugated onto the AuNP having 20 nm size through the thiol-gold coordinate bonding. Successful construction of the nanoarchitecture uPIC-AuNPs was achieved by the preformation of uPICs and the stable bonding between uPICs and AuNP. The size of generated uPIC-AuNPs was precisely controlled in the range of less than 50 nm by the sizes of nanotemplate AuNP and surrounding uPICs. The uPIC-AuNPs efficiently delivered siRNA into cultured cancer cells, allowing the significant sequence-specific gene silencing without apparent cytotoxicity. The systemically administered uPIC-AuNPs showed much longer blood circulation property and significantly enhanced accumulation of siRNA in a subcutaneous cervical cancer model, compared to their component controls (bare AuNPs and uPICs). Ultimately, uPIC-AuNPs achieved the significant gene silencing in the tumor tissue through systemic administration. These results demonstrate the potential of uPIC-conjugated nanoarchitectures for systemic siRNA delivery toward RNAi-based cancer therapy.

## MATERIALS AND METHODS

**Materials.** ε-Trifluoroacetyl-L-lysine *N*-carboxy anhydride (Lys(TFA)-NCA) was prepared by the Fuchs–Farthing method using triphosgene.[35] α-Methoxy-ω-amino PEG (PEG-$NH_2$, $M_n$ = 2200) was obtained from NOF Co., Ltd. (Tokyo, Japan). *N*,*N*-Dimethylformamide (DMF) was purchased from Wako Pure Chemical Industries, Ltd. (Osaka, Japan). Dithiothreitol (DTT), dimethyl sulfoxide (DMSO), diisopropylethylamine (DIPEA), and Dulbecco's modified Eagle's media (DMEM) were purchased from Sigma-Aldrich Co. (St. Louis, MO, USA). DMSO, DMF, and DIPEA were purified by distillation under reduced pressure. Gold nanoparticle (20 nm in diameter) was purchased from BBInternational (Cardiff, UK). Succinimidyl 6-[3-(2-pyridyldithio)-propionamido]hexanoate (LC-SPDP) was obtained from Pierce (Rockford, IL, USA). Hepes (1 M, pH 7.3) was purchased from Amresco (Solon, OH, USA). The luciferase-expressing human cervical cancer cell line, HeLa-Luc, was purchased from Caliper LifeScience (Hopkinton, MA, USA). Fetal bovine serum was provided by Dainippon Sumitomo Pharma Co., Ltd. (Osaka, Japan). BALB/c nude and BALB/c mice were purchased from Charles River Japan (Kanagawa, Japan). siRNAs were synthesized by Hokkaido System Science Co., Ltd. (Hokkaido, Japan), and the sequences used are as follows: (1) Firefly GL3 luciferase (siLuc): 5′-CUU ACG CUG AGU ACU UCG AdTdT-3′ (sense), 5′-UCG AAG UAC UCA GCG UAA GdTdT-3′ (antisense); (2) control (siCont): 5′-UUC UCC GAA CGU GUC ACG UdTdT-3′ (sense), 5′-ACG UGA CAC GUU CGG AGA AdTdT-3′ (antisense). All dyes (Alexa647 and Cy3) were attached to 5′-end of sense stand of siLuc. All animal experiments were carried out in accordance with the guidelines for animal experiments at The University of Tokyo, Japan.

**Synthesis of PEG-PLL(TFA).** PEG-PLL(TFA) was prepared by ring-opening polymerization of Lys(TFA)-NCA, as previously described.[35] Briefly, Lys(TFA)-NCA (1 g, 3.7 mmol) was dissolved in DMSO (40 mL). After the addition of the macroinitiator PEG-$NH_2$ (176 mg, 88.8 μmol) to DMSO (7.0 mL), the reaction solution was stirred at 25 °C for 72 h under Ar. The resulting solution was precipitated into an excess amount of diethyl ether and dried *in vacuo*. The prepared PEG-PLL(TFA) was characterized by gel permeation chromatography (GPC) and $^1$H NMR (400 MHz, ECS-400, JEOL, Tokyo, Japan). The DP of Lys(TFA) units was calculated to be 38 in the $^1$H NMR spectrum from the peak intensity ratio of the β, γ, and δ-methylene protons of lysine ($-(CH_2)_3-$, $\delta$ = 1.4–1.8) to the oxyethylene protons of PEG ($-(OCH_2CH_2)-$, $\delta$ = 3.7). The GPC system (HLC-8220, TOSOH CORPORATION, Tokyo, Japan) equipped with two TSK gel columns (TSK-gel Super AW4000 and Super AW3000) was eluted with DMF containing lithium chloride (10 mM) at 0.8 mL/min. Molecular weight distribution ($M_w/M_n$) of the block copolymer was determined to be 1.07.

**Synthesis of PEG-PLL(TFA)-LC-SPDP.** PEG-PLL(TFA) (46.5 mg, 4.47 μmol) was dissolved in DMF (2 mL) and stirred overnight at 40 °C under Ar. LC-SPDP (20.5 mg, 44.7 μmol) in DMF (1 mL) was added to the polymer solution and further stirred at 35 °C for 4 h. DIPEA (4 μL, 22.4 μmol) in DMF (0.4 mL) was added to the reacting solution and stirred overnight. The resulting solution was dialyzed against methanol and then deionized water, followed by lyophilization. The prepared PEG-PLL(TFA)-LC-SPDP was characterized in MeOD at 40 °C by $^1$H NMR (400 MHz, ECS-400) from the peak intensity ratio of the methylene protons of dithiopropionyl group ($-COCH_2CH_2SS-$, $\delta$ = 2.3) to the oxyethylene protons of PEG ($-(OCH_2CH_2)-$, $\delta$ = 3.7). The conjugation ratio of LC-SPDP was calculated to be ~70%.

**Deprotection of TFA and Pyridyl Groups.** PEG-PLL(TFA)-LC-SPDP (20 mg) was dissolved in a mixed solvent of methanol (9 mL) and 1 N NaOH solution (1 mL), and then reacted at 35 °C for 8 h. The mixture was dialyzed against 0.01 N HCl and then deionized water. The final solution was lyophilized to obtain PEG-PLL-LC-SPDP in the chloride salt form. The deprotection of the TFA groups was confirmed in $D_2O$ at 80 °C by $^1$H NMR (400 MHz, ECS-400) from the peak shift of the ε-methylene protons from 3.0 to 3.3 ppm. For deprotection of pyridyl group, PEG-PLL-LC-SPDP (9 mg) was incubated with DTT (0.8 mg) at ambient temperature for 1 h in 10 mM sodium phosphate buffer (pH 7.2). The solution was dialyzed against 0.01 N HCl containing 1 mM EDTA for 2 h, 1 mM EDTA for 1 h, and then deionized water at 4 °C for 1 h. Finally, the product was lyophilized to obtain PEG-PLL-SH. Deprotection of pyridyl group was confirmed by Ellman's assay (data not shown).

**Preparation of Single siRNA-Loaded uPICs and uPIC-installed Gold Nanoparticle (uPIC-AuNP).** PEG-PLL-SH and siRNA were separately

dissolved in 10 mM Hepes buffer (pH 7.2) and mixed at varying molar ratios of PEG-PLL-SH to siRNA ([PEG-PLL-SH]/[siRNA]) to form uPICs (siRNA concentration: 17 $\mu$M). The uPIC solution was incubated for 1 h at ambient temperature. AuNP solution was concentrated to 60 nM by centrifugation (14 000 rpm, 10 min) in 20 $\mu$L and mixed with uPIC solution at a molar ratio of siRNA to AuNP ([siRNA]/[AuNP]) = 360. 10 mM Hepes buffer (pH 7.2) was added to the mixture for maintaining pH at 7.2, followed by 8 h incubation at 4 °C. Then, 2 M NaCl was added to the solution (final NaCl concentration: 150 mM). The solution was further incubated for 8 h. Unbound uPICs were removed by repeated centrifugations in 10 mM Hepes buffer (pH 7.2) containing 150 mM NaCl (14,000 rpm, 10 min). Finally, the uPIC-AuNPs were dispersed in 10 mM Hepes buffer (pH 7.2) containing 150 mM NaCl (AuNP concentration: 11 nM).

**Diffusion Coefficient Measurements by Fluorescence Correlation Spectroscopy (FCS).** FCS analyses were performed using a LSM510 confocal laser scanning microscope (CLSM, Carl Zeiss, Oberlochen, Germany) equipped with the Zeiss C-Apochromat 40× water objective and Confocor3 module. A He–Ne laser (543 nm) was used for Cy3-siRNA excitation and emission was obtained through a 560–615 nm band-pass filter. Samples were placed into 8-well Lab-Tek chambered borosilicate cover glass (Nalge Nunc International, Rochester, NY, USA) and measured at ambient temperature. The uPIC stability was evaluated in 10 mM Hepes buffer (pH 7.2) with or without 150 mM NaCl, as well as PBS containing 10% FBS. The uPICs prepared at 5 $\mu$M Cy3-siRNA were diluted with each media up to 10 nM Cy3-siRNA. After overnight incubation at 37 °C, the measurements were carried out with a sampling time of 10 s (10 measurements). The obtained autocorrelation curves were fitted with the Zeiss Confocor3 software package to calculate the diffusion coefficient.

**Measurement of Molecular Weight (MW) of PICs by Analytical Ultracentrifuge (AUC).** MW of PICs ($MW_{PIC}$) was determined by sedimentation equilibrium experiments with AUC equipped with absorbance optics (Beckman Coulter, CA, USA). The PIC solution was diluted up to 0.6 $\mu$M siRNA concentration with 10 mM Hepes buffer (pH 7.2) containing 150 mM NaCl. Absorbance at 260 nm was measured as a function of centrifugal radius ($r$) at 20 °C, and the obtained data was analyzed by ORIGIN software (Beckman Coulter, CA, USA) to determine the $MW_{PIC}$ by the following equation based on the values of partial specific volume of PICs ($PSV_{PIC}$) and the buffer density.

$$\ln(C(r)/C(r_0)) = MW_{PIC} \times (1 - PSV_{PIC} \times \rho_0) \times \omega^2 \times (r^2 - r_0^2)/2RT$$

where $C(r)$ is a concentration of siRNA at $r$, $\omega$ is rotational speed, $R$ is the gas constant, $T$ is the temperature, and $C(r_0)$ is a concentration of siRNA at a reference radial distance. $PSV_{PIC}$ was determined as a mass average of $PSV_{siRNA}$ and $PSV_{PEG\text{-}PLL}$.

$$PSV_{PIC} = (M_{PEG\text{-}PLL} \times PSV_{PEG\text{-}PLL} + M_{siRNA} \times PSV_{siRNA})/(M_{PEG\text{-}PLL} + M_{siRNA})$$

where $M_{PEG\text{-}PLL}$ and $M_{siRNA}$ are the mass of PEG-PLL and siRNA, respectively, in the solution. Each value was calculated from the density of siRNA or PEG-PLL solution measured by a density meter DMA4500/DMA5000 (Anton Paar, Graz, Austria). All the siRNA and PEG-PLL solutions were diluted up to 1, 2, and 5 mg/mL with 10 mM Hepes buffer (pH 7.2) containing 150 mM NaCl, and then the density measurements were performed at 20 °C. The PSV of component $i$ ($PSV_i$) was calculated from the following equation:

$$PSV_i = (1 - d\rho/dc)/\rho_0$$

where $\rho_0$ is the density of buffer, $\rho$ is the density of solution, and $c$ is the concentration of solute. From the experiments, $PSV_{PIC}$ and $MW_{PIC}$ were determined to be 0.602 $cm^3/g$ and 22 000 g/mol, respectively.

**Physicochemical Characterizations of uPIC-AuNPs.** UV–vis absorbance spectra of uPIC-AuNPs and the other control samples at 12 nM AuNP were measured using NanoDrop (Thermo Fisher Scientific Inc., Waltham, MA, USA). Sample sizes were determined at 25 °C by dynamic light scattering (DLS) method using a Zetasizer (Malvern Instruments Ltd., Worcestershire, UK) equipped with a He–Ne laser ($\lambda$ = 633 nm) as the incident beam at a detection angle of 173°. The data obtained from the rate of decay in the photon correlation function were analyzed by the histogram method. Zeta-potentials of samples were also determined using the same apparatus.

**Transmission Electron Microscopy (TEM) Observation.** The morphologies of AuNPs and uPIC-AuNPs were examined using a TEM (JEM-1400, JEOL, Tokyo, Japan) at an acceleration voltage of 100 kV and a beam current of 40 $\mu$A. Each sample was stained with uranyl acetate solution (2 w/v%) and placed on 400-mesh copper grids.

**Gel Electrophoresis.** uPIC or uPIC-AuNP solution was mixed with heparin and GSH, and the mixtures were incubated for 10 min at room temperature (siRNA: 400 nM, heparin: 0, 1, 2, and 3 $\mu$g/mL, GSH: 0 and 10 mM). Then, the mixtures were analyzed by gel electrophoresis (1% agarose, 1 × TBE buffer, 100 V, 15 min). After staining with SYBR Green II, the band from siRNA was detected using a Molecular Imager FX (BIO-RAD) (Ex/Em: 488/530 nm) equipped with Quantity One software (BIO-RAD). In the other experiments, (i) uPIC solutions were incubated with GSH for 15 min at room temperature (GSH concentrations; 0, 10, 20, 30, and 50 mM), (ii) AuNP solutions were treated with 10 mM GSH or 10 mM cysteine for 10 min at room temperature, and then mixed with uPIC solutions, followed by additional incubation for 10 min (siRNA: 400 nM, AuNP: 0, 2, 4, and 10 nM), and (iii) AuNPs were treated with 10 mM cysteine or 10 mM GSH for 10 min at room temperature (AuNP: 4 nM).

***In Vitro* Luciferase Assay.** HeLa-Luc cells were seeded on a 96-well plate at a density of 5000 cells/well in DMEM containing 10% FBS (DMEM/FBS). siLuc or siCont-loaded uPIC-AuNPs were added to the cells and incubated for 48 h. Next, the cells were lysed using the cell lysis buffer (Promega, Fitchburg, WI, USA). Luminescence intensities of cell lysates were measured using the Luciferase Assay System (Promega) on a luminescence microplate reader (Mithras LB 940, Berthold technologies, Bad Wildbad, Germany). The relative luciferase activity was determined by normalizing the luminescence intensity of the sample-treated lysates to the amount of proteins contained in the lysates (determined using a BCA assay kit), followed by further normalization to buffer-treated controls ($n$ = 4).

**Flow Cytometric Analysis.** HeLa-Luc cells were seeded on a 6-well plate at a density of 100 000 cells/well in DMEM/FBS. uPIC-AuNPs or uPICs prepared with Alexa647-labeled siRNA were added to the cells at 200 nM siRNA. After 24 h incubation, the media was removed and the cells were washed with cold PBS twice. The cells were treated with a trypsin-EDTA solution for 2 min and then suspended in cold PBS. The fluorescence intensity of Alexa647-labeled siRNA from the cells was measured using a BD LSR II (BD Biosciences, San Jose, CA, USA). The cells treated with 10 mM Hepes buffer (pH 7.2) containing 150 mM NaCl were used as a control.

**Confocal Laser Scanning Microscopic (CLSM) Observation.** HeLa-Luc cells were seeded on a 35 mm glass-based dish (Iwaki, Tokyo, Japan) at a density of 50 000 cells/well in DMEM/FBS. The uPIC-AuNPs loading Alexa647-labeled siRNA were added to the cells at 200 nM siRNA. After 24 h incubation, the culture media was removed and the cells were washed with cold PBS twice. Each dish was observed using a CLSM (LSM 510, Carl Zeiss) equipped with a Zeiss C-Apochromat 63× objective (Carl Zeiss). The excitation wavelength was set at 633 nm (He–Ne laser) for Alexa647-labeled siRNA, and the emission was detected between 651 and 704 nm.

**Quantification of Blood Circulation of uPIC-AuNPs.** siCont-loaded uPIC-AuNPs were intravenously injected (AuNP: 3.3 × $10^{12}$ particles/mouse, siRNA: 1.4 $\mu$g/mouse) into the tail vein of mice (BALB/c, female, 8 week old). The mice were sacrificed at a designated time and the collected blood was centrifuged (1500 rpm, 3 min) to obtain the plasma (20 $\mu$L). The plasma was treated with 90% $HNO_3$ by heating and stored in 1% $HNO_3$ solution overnight. The resulting sample solution was filtered using a 0.45 $\mu$m pore size membrane filter and further diluted to a desired concentration using 1% $HNO_3$ solution. The Au content was determined by ICP-MS (7700 Series, Agilent Technologies, Santa Clara, CA, USA).

**Accumulation of uPIC-AuNPs in a Subcutaneous HeLa-Luc Tumor.** Tumor accumulation of uPIC-AuNPs was determined in mice bearing a subcutaneous HeLa-Luc tumor. Tumors were prepared by injecting $5 \times 10^6$ cells under the skin in the left rear flank of mice (BALB/c nude, female, 8 week old), and were allowed to mature for 2 weeks ($n = 4$). Mice were fed with an alfalfa-free chow for 2 weeks before sample injection. uPIC-AuNPs or the other control samples (naked siRNA, uPICs, and the mixture of uPICs without thiol and AuNPs) prepared with Alexa647-labeled siRNA were injected into the tail vein of mice (4.8 $\mu$g siRNA/mouse). After 4 h, mice were sacrificed and tumor was excised. The excised tumor was imaged using an IVIS instrument (Caliper LifeScience, Hopkinton, MA, USA) in the fluorescence mode with appropriate filters for excitation (640 nm) and emission (720 nm). Data were analyzed using Living Image software (Caliper LifeScience) by drawing ROIs around the tumor to determine the fluorescence intensity and normalized with the background signal from nontreated tumors. Accumulation of siRNA in the tumor was expressed as an average of fluorescence intensity/tumor area.

***In Vivo* Luciferase Assay in Subcutaneous HeLa-Luc Tumor.** *In vivo* luciferase gene silencing ability was determined for mice bearing subcutaneous HeLa-Luc tumors, following the scheme shown in Figure S9A (SI). Tumors were prepared by injecting $5 \times 10^6$ cells under the skin in the right rear flank of mice (BALB/c nude, female, 8 week old) at day 0. The uPIC-AuNPs containing siLuc or siCont were intravenously injected into the tail vein of mice at days 17 and 18 (5.8 $\mu$g siRNA/mouse/shot). The luminescence intensity (IL) from the tumors was measured at days 17, 18, and 19 by an IVIS instrument equipped with a Living Image software (PerkinElmer). The luciferase gene silencing ability of uPIC-AuNPs was estimated from an increasing rate of LI ($IR_{LI}$) associated with the tumor growth. By assuming that the LI from the tumor should be proportional to the tumor volume (or the number of cancer cells), the $IR_{LI}$ can be expressed as $\ln(LI_{t+1}/LI_t)$, where $LI_t$ is the luminescence intensity from the tumor at day $t$, according to the calculating formula of the growth rate of tumor (GR): $GR = \ln(V_{t+1}/V_t)$, where $V_t$ is the tumor volume at day $t$.[36] The $IR_{LI}$ values between days 17 and 18 (after first injection), and days 18 and 19 (after second injection) were calculated using the LI measured at each day (Figure S9B (SI)), and further averaged to estimate the overall $IR_{LI}$, *i.e.*, $[\ln(LI_{18}/LI_{17}) + \ln(LI_{19}/LI_{18})]/2$, as an indicator of luciferase gene silencing activity (Figure 6C).

*Conflict of Interest:* The authors declare no competing financial interest.

*Acknowledgment.* This research was financially supported by the Funding Program for World-Leading Innovative R&D in Science and Technology (FIRST) (JSPS), Grants-in-Aid for Scientific Research of MEXT (JSPS KAKENHI Grant Numbers 25000006 and 25282141), the Center of Innovation (COI) Program (JST), Grants-in-Aid for Scientific Research of MHLW, and National Institute of Biomedical Innovation. H. J. Kim would like to thank A. Kim for his help with the TEM imaging of gold nanoparticles and also S. Chuanoi for his assistance with polymer synthesis.

*Supporting Information Available:* $^1$H NMR of PEG-PLL-SH, TEM image of bare AuNPs, fluorescence intensity plotted against various uPIC concentrations, viability of HeLa-Luc cells treated with uPIC-AuNPs or uPICs, CLSM images of HeLa-Luc cells treated with uPICs. This material is available free of charge *via* the Internet at http://pubs.acs.org.

## REFERENCES AND NOTES

1. Aagaard, L.; Rossi, J. J. RNAi Therapeutics: Principles, Prospects and Challenges. *Adv. Drug Delivery Rev.* **2007**, *59*, 75–86.
2. Burnett, J. C.; Rossi, J. J. RNA-Based Therapeutics: Current Progress and Future Prospects. *Chem. Biol.* **2012**, *19*, 60–71.
3. Dykxhoorn, D. M. RNA Interferences as an Anticancer Therapy: a Patent Perspective. *Expert Opin. Ther. Pat.* **2009**, *19*, 475–491.
4. He, S.; Zhang, D.; Cheng, F.; Gong, F.; Guo, Y. Applications of RNA Interference in Cancer Therapeutics as a Powerful Tool for Suppressing Gene Expression. *Mol. Biol. Rep.* **2009**, *36*, 2153–2163.
5. Nishiyama, N.; Kataoka, K. Current State, Achievements, and Future Prospects of Polymeric Micelles as Nanocarriers for Drug and Gene Delivery. *Pharmacol. Ther.* **2006**, *112*, 630–648.
6. Lee, Y.; Kataoka, K. Biosignal-Sensitive Polyion Complex Micelles for the Delivery of Biopharmaceuticals. *Soft Matter* **2009**, *5*, 3810–3817.
7. Guo, X.; Huang, L. Recent Advances in Nonviral Vectors for Gene Delivery. *Acc. Chem. Res.* **2012**, *45*, 971–979.
8. Wagner, E. Polymers for siRNA Delivery: Inspired by Viruses to be Targeted, Dynamic, and Precise. *Acc. Chem. Res.* **2012**, *45*, 1005–1013.
9. Nakase, I.; Akita, H.; Kogure, K.; Graslund, A.; Langel, U.; Harashima, H.; Futaki, S. Efficient Intracellular Delivery of Nucleic Acid Pharmaceuticals Using Cell-Penetrating Peptides. *Acc. Chem. Res.* **2012**, *45*, 1132–1139.
10. Kanasty, R. L.; Whitehead, K. A.; Vegas, A. J.; Anderson, D. G. Action and Reaction: the Biological Response to siRNA and Its Delivery Vehicles. *Mol. Ther.* **2012**, *20*, 513–524.
11. Matsumura, Y.; Maeda, H. A New Concept for Macromolecular Therapeutics in Cancer Chemotherapy: Mechanism of Tumoritropic Accumulation of Proteins and the Antitumor Agent Smancs. *Cancer Res.* **1986**, *46*, 6387–6392.
12. Maeda, H. Macromolecular Therapeutics in Cancer Treatment: the EPR Effect and Beyond. *J. Controlled Release* **2012**, *164*, 138–144.
13. Cabral, H.; Matsumoto, Y.; Mizuno, K.; Chen, Q.; Murakami, M.; Kimura, M.; Terada, Y.; Kano, M. R.; Miyazono, K.; Uesaka, M.; *et al.* Accumulation of Sub-100 nm Polymeric Micelles in Poorly Permeable Tumors Depends on Size. *Nat. Nanotechnol.* **2011**, *6*, 815–823.
14. Tang, L.; Fan, T. M.; Borst, L. B.; Cheng, J. Synthesis and Biological Response of Size-Specific, Monodisperse Drug-Silica Nanoconjugates. *ACS Nano* **2012**, *6*, 3954–3966.
15. Harada, A.; Kataoka, K. Chain Length Recognition: Core-Shell Supramolecular Assembly from Oppositely Charged Block Copolymers. *Science* **1999**, *283*, 65–67.
16. DeRouchey, J.; Schmidt, C.; Walker, G. F.; Koch, C.; Plank, C.; Wagner, E.; Radler, J. O. Monomolecular Assembly of siRNA and Poly(ethylene glycol)-Peptide Copolymers. *Biomacromolecules* **2008**, *9*, 724–732.
17. Shimizu, H.; Hori, Y.; Kaname, S.; Yamada, K.; Nishiyama, N.; Matsumoto, S.; Miyata, K.; Oba, M.; Yamada, A.; Kataoka, K.; *et al.* siRNA-Based Therapy Ameliorates Glomerulonephritis. *J. Am. Soc. Nephrol.* **2010**, *21*, 622–633.
18. Rosi, N. L.; Mirkin, C. A. Nanostructures in Biodiagnostics. *Chem. Rev.* **2005**, *105*, 1547–1562.
19. Nel, A. E.; Madler, L.; Velegol, D.; Xia, T.; Hoek, E. M. V.; Somasundaran, P.; Klaessig, F.; Castranova, V.; Thompson, M. Understanding Biophysicochemical Interactions at the Nano-Bio Interface. *Nat. Mater.* **2009**, *8*, 543–557.
20. Saito, G.; Swanson, J. A.; Lee, K.-D. Drug Delivery Strategy Utilizing Conjugation *via* Reversible Disulfide Linkages: Role and Site of Cellular Reducing Activities. *Adv. Drug Delivery Rev.* **2003**, *55*, 199–215.
21. Buyens, K.; Meyer, M.; Wagner, E.; Demeester, J.; De Smedt, S. C.; Sanders, N. N. Monitoring the Disassembly of siRNA Polyplexes in Serum is Crucial for Predicting Their Biological Efficacy. *J. Controlled Release* **2010**, *141*, 38–41.
22. Kim, H. J.; Ishii, A.; Miyata, K.; Lee, Y.; Wu, S.; Oba, M.; Nishiyama, N.; Kataoka, K. Introduction of Stearoyl Moieties into a Biocompatible Cationic Polyaspartamide Derivative, PAsp(DET), with Endosomal Escaping Function for Enhanced siRNA-Mediated Gene Knockdown. *J. Controlled Release* **2010**, *145*, 141–148.
23. Rana, T. M. Illuminating the Silence: Understanding the Structure and Function of Small RNAs. *Nat. Rev. Mol. Cell Biol.* **2007**, *8*, 23–36.
24. Abels, J. A.; Moresno-Herrero, F.; Van der Heijden, T.; Dekker, C.; Dekker, N. H. Single-Molecule Measurements

of the Persistence Length of Double-Stranded RNA. *Biophys. J.* **2005**, *88*, 2737–2744.
25. Kenausis, G. L.; Voros, J.; Elbert, D. L.; Huang, N.; Hofer, R.; Ruiz-Taylor, L.; Textor, M.; Hubbell, J. A.; Spencer, N. D. Poly(L-lysine)-g-Poly(ethylene glycol) Layers on Metal Oxide Surfaces: Attachment Mechanism and Effects of Polymer Architecture on Resistance to Protein Adsorption. *J. Phys. Chem. B* **2000**, *104*, 3298–3309.
26. Giljohann, D. A.; Seferos, D. S.; Prigodich, A. E.; Patel, P. C.; Mirkin, C. A. Gene Regulation with Polyvalent siRNA-Nanoparticle Conjugates. *J. Am. Chem. Soc.* **2009**, *131*, 2072–2073.
27. Zuckerman, J. E.; Choi, C. H. J.; Han, H.; Davis, M. E.; Polycation-siRNA Nanoparticles, Can Disassemble at the Kidney Glomerular Basement Membrane. *Proc. Natl. Acad. Sci. U. S. A.* **2012**, *109*, 3137–3142.
28. Lee, J.-S.; Green, J. J.; Love, K. T.; Sunshine, J.; Langer, R.; Anderson, D. G. Gold, Poly($\beta$-amino ester) Nanoparticles for Small Interfering RNA Delivery. *Nano Lett.* **2009**, *9*, 2403–2406.
29. Mislick, K. A.; Baldeschwieler, J. D. Evidence for the Role of Proteoglycans in Cation-Mediated Gene Transfer. *Proc. Natl. Acad. Sci. U. S. A.* **1996**, *93*, 12349–12354.
30. Chithrani, D. B. Intracellular Uptake, Transport, and Processing of Gold Nanostructures. *Mol. Membr. Biol.* **2010**, *27*, 299–311.
31. Seymour, L. W.; Duncan, R.; Strohalm, J.; Kopecek, J. Effect of Molecular Weight (Mw) of *N*-(2-Hydroxypropyl)-methacrylamide Copolymers on Body Distribution and Rate of Excretion After Subcutaneous, Intraperitoneal, and Intravenous Administration to Rats. *J. Biomed. Mater. Res.* **1987**, *21*, 1341–1358.
32. Matsumoto, Y.; Nomoto, T.; Cabral, H.; Matsumoto, Y.; Watanabe, S.; Christie, R. J.; Miyata, K.; Oba, M.; Ogura, T.; Yamasaki, Y.; *et al.* Direct and Instantaneous Observation of Intravenously Injected Substances Using Intravital Confocal Micro-Videography. *Biomed. Opt. Express* **2010**, *1*, 1209–1216.
33. Kim, H. J.; Oba, M.; Pittella, F.; Nomoto, T.; Cabral, H.; Matsumoto, Y.; Miyata, K.; Nishiyama, N.; Kataoka, K. PEG-Detachable Cationic Polyaspartamide Derivatives Bearing Stearoyl Moieties for Systemic siRNA Delivery toward Subcutaneous BxPC3 Pancreatic Tumor. *J. Drug Targeting* **2012**, *20*, 33–42.
34. Nomoto, T.; Matsumoto, Y.; Miyata, K.; Oba, M.; Fukushima, S.; Nishiyama, N.; Yamasoba, T.; Kataoka, K. *In Situ* Quantitative Monitoring of Polyplexes and Polyplex Micelles in the Blood Circulation Using Intravital Real-Time Confocal Laser Scanning Microscopy. *J. Controlled Release* **2011**, *151*, 104–109.
35. Harada, A.; Kataoka, K. Formation of Polyion Complex Micelles in an Aqueous Milieu from a Pair of Oppositely-Charged Block Copolymers with Poly(ethylene glycol) Segments. *Macromolecules* **1995**, *28*, 5294–5299.
36. Mehrara, E.; Forssell-Aronsson, E.; Ahlman, H.; Bernhardt, P. Quantitative Analysis of Tumor Growth Rate and Changes in Tumor Marker Level: Specific Growth Rate *Versus* Doubling Time. *Acta Oncol.* **2009**, *48*, 591–597.

Macromolecular Journals

Macromolecular Rapid Communications

# Fine-Tuning of Charge-Conversion Polymer Structure for Efficient Endosomal Escape of siRNA-Loaded Calcium Phosphate Hybrid Micelles

Yoshinori Maeda, Frederico Pittella, Takahiro Nomoto, Hiroyasu Takemoto, Nobuhiro Nishiyama, Kanjiro Miyata,* Kazunori Kataoka*

For efficient delivery of siRNA into the cytoplasm, a smart block copolymer of poly(ethylene glycol) and charge-conversion polymer (PEG-CCP) is developed by introducing 2-propionic-3-methylmaleic (PMM) amide as an anionic protective group into side chains of an endosome-disrupting cationic polyaspartamide derivative. The PMM amide moiety is highly susceptible to acid hydrolysis, generating the parent cationic polyaspartamide derivative at endosomal acidic pH 5.5 more rapidly than a previously synthesized *cis*-aconitic (ACO) amide control. The PMM-based polymer is successfully integrated into a calcium phosphate (CaP) nanoparticle with siRNA, constructing PEGylated hybrid micelles (PMM micelles) having a sub-100 nm size at extracellular neutral pH 7.4. Ultimately, PMM micelles achieve the significantly higher gene silencing efficiency in cultured cancer cells, compared to ACO control micelles, probably due to the efficient endosomal escape of the PMM micelles. Thus, it is demonstrated that fine-tuning of acid-labile structures in CCP improves the delivery performance of siRNA-loaded nanocarriers.

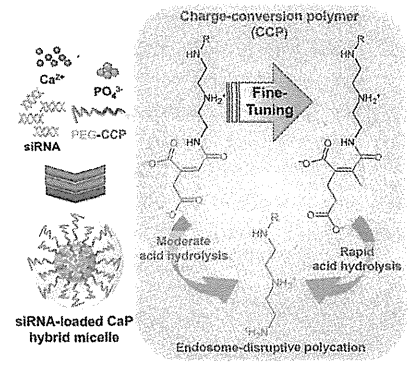


Y. Maeda, T. Nomoto, Prof. K. Kataoka
Department of Bioengineering, Graduate School of Engineering, The University of Tokyo, 7–3–1 Hongo, Bunkyo-ku, Tokyo 113–8656, Japan
E-mail: kataoka@bmw.t.u-tokyo.ac.jp
Dr. F. Pittella, Dr. K. Miyata, Prof. K. Kataoka
Center for Disease Biology and Integrative Medicine, Graduate School of Medicine, The University of Tokyo, 7–3–1 Hongo, Bunkyo-ku, Tokyo 113–0033, Japan
E-mail: miyata@bmw.t.u-tokyo.ac.jp
Dr. H. Takemoto, Prof. N. Nishiyama
Polymer Chemistry Division, Chemical Resources Laboratory, Tokyo Institute of Technology, R1–11, 4259 Nagatsuta, Midori-ku, Yokohama 226–8503, Japan
Prof. K. Kataoka
Department of Materials Engineering, Graduate School of Engineering, The University of Tokyo, 7–3–1 Hongo, Bunkyo-ku, Tokyo 113–8656, Japan

## 1. Introduction

Small interfering RNA (siRNA) has been greatly highlighted as a potential therapeutic agent for a variety of intractable diseases, including cancer.[1] To obtain therapeutic benefits, siRNA needs to be transported to the cytoplasm after cellular internalization. However, endocytosed macromolecules are generally entrapped by acidic vesicular compartments, i.e., endosomes, within cells, leading to the lysosomal degradation.[2] Hence, various polymeric materials have been developed to facilitate endosome disruption for smooth endosomal escape of siRNA.[3] Polyethylenimine (PEI) is one of the most widely used polymers for the endosomal escape of nucleic acids. It is believed that the low $pK_a$ amines in PEI can serve as a proton sponge in acidic endosomes (pH ≈ 5.5) to

*Macromol. Rapid Commun.* **2014**, *35*, 1211–1215


DOI: 10.1002/marc.201400049

induce endosome disruption,[4,5] due to the increased osmotic pressure within the vesicles and/or the direct interactions of highly charged PEI with oppositely charged endosomal membrane.[6,7] However, significantly protonated PEI even under extracellular conditions (pH 7.4) concurrently induces the considerable cytotoxicity due to the cytoplasmic membrane damage.[8,9] Therefore, further development of endosome-disrupting polymers is still demanded for more efficient, yet less toxic endosomal escape of siRNA.

Our previous studies revealed that diaminoethane unit (—$NHCH_2CH_2NH$—) showed a distinctive change in the protonated state between pH 7.4 and 5.5, i.e., the monoprotonated state at pH 7.4 and the diprotonated state at pH 5.5.[10,11] Accordingly, a polyaspartamide derivative bearing the diaminoethane unit in the side chain, poly{*N*′-[*N*-(2-aminoethyl)-2-aminoethyl]aspartamide} (PAsp(DET)), successfully induced acidic pH-responsive membrane destabilization because of the change in its protonated state.[11–14] PAsp(DET) allowed efficient gene expression of plasmid DNA in cultured cells, associated with significantly lower cytotoxicity compared to PEI.[10–14] Meanwhile, primary amines in PAsp(DET) could be further modified with *cis*-aconitic (ACO) anhydride to generate an endosome-disrupting polyanion PAsp(DET-ACO), where ACO amide was subjected to acid hydrolysis for regeneration of the parent polycation PAsp(DET).[15] Thus, this polyanion was termed the charge-conversion polymer (CCP) based on its charge-conversion from the negative to the positive at acidic pH.

This CCP-based strategy was quite useful for siRNA delivery, when a block copolymer of poly(ethylene glycol) and CCP (PEG–CCP) was applied for construction of hybrid micelles with calcium phosphate (CaP) precipitates (Figure S1, Supporting Information).[16–18] CaP precipitates have been extensively used as a conventional transfection reagent of nucleic acids, because of their extremely low-cost and simple preparation scheme. However, the rapid growth of CaP crystal has substantially hampered the utilization of CaP precipitates for systemic nucleic acid delivery.[19] In this regard, PEG–CCP provided CaP precipitates with a PEG shell for size-controlling as well as biocompatibility to form monodispersive hybrid polymeric micelles. Indeed, siRNA-loaded hybrid micelles were prepared with CaP and PEG–CCP, having a size of sub-100 nm with a narrow size distribution, and induced efficient gene silencing in various cultured cancer cells.[16–18] Ultimately, systemically administered hybrid micelles showed the significant antitumor activity in a subcutaneous pancreatic cancer model by delivering the siRNA targeted for vascular endothelial growth factor.[17]

In our previous studies, the ACO amide, which is a maleic acid derivative bearing 2-acetic acid moiety, has been utilized as an acid-labile bond (Figure 1). It is known in this regard that the sensitivity of maleic acid amides to acid hydrolysis can be altered by functional groups substituted at the 2- and 3-positions of the maleic acid amide.[20] Indeed, 2-propionic-3-methyl maleic (PMM) amide was demonstrated to be more susceptible to acid hydrolysis compared to ACO amide.[21] This fact motivated us to finely tune the acid-labile amide structure in PEG–CCP for improving the endosome-escaping functionality. In the present study, a second generation of PEG–CCP was newly synthesized by introducing the PMM moieties into primary amines in PEG–PAsp(DET). The obtained block copolymer PEG–PAsp(DET-PMM) was compared with PEG-PAsp(DET-ACO) in terms of the sensitivity to acid hydrolysis and the delivery efficacy based on the hybrid micelle formulation.

## 2. Experimental Section

All experimental details are described in Supporting Information.

## 3. Results and Discussion

siRNA and its nanocarriers, once internalized into cells, are transported to the late endosomes (or the lysosomes),

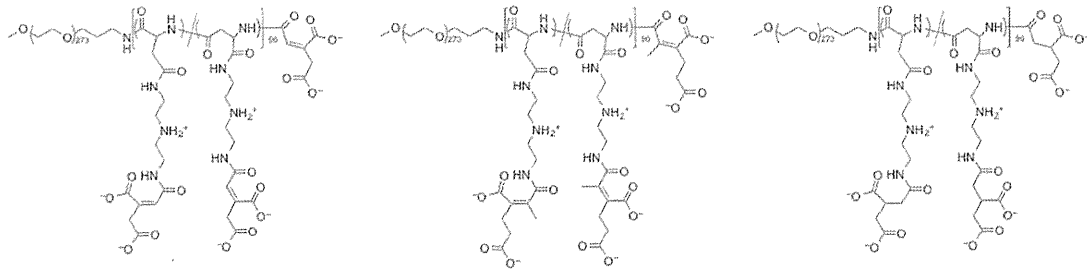


*Figure 1.* Chemical structures of PEG-PAsp(DET-ACO) and PEG-PAsp(DET-PMM) as PEG-CCPs, and PEG-PAsp(DET-CAR) as a PEG-nonCCP. The carballylic (CAR) moiety is a succinic acid derivative, and thus, its amide is much less sensitive to acid hydrolysis, compared to the maleic acid derivatives, PMM and ACO moieties.

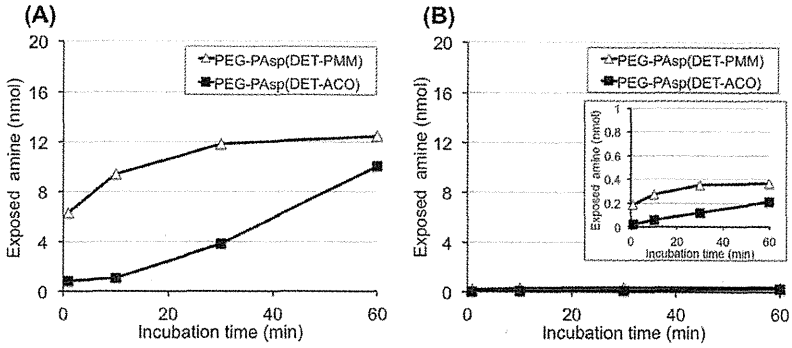


*Figure 2.* Amount of exposed amine in PEG–PAsp(DET–PMM) and PEG–PAsp(DET–ACO) after incubation at A) pH 5.5 and B) pH 7.4. The amount of exposed amine was determined from standard curves prepared with glycine solutions in an acetate buffer (pH 5.5) and a phosphate buffer (pH 7.4).

followed by lysosomal degradation.[2,22] Thus, they need to escape from those vesicular compartments to the cytoplasm before degrading for exerting gene silencing effect. Here, a smart block copolymer of biocompatible PEG and endosome-disrupting PAsp(DET–PMM) was synthesized by introducing a PMM moiety into primary amines in PAsp(DET) side chains through the amide bond formation (Figure 1 and Scheme S1, Supporting Information). It is reported that PMM amide is cleaved more rapidly than ACO amide in acidic conditions, probably because the $pK_a$ value of carboxylates in dimethylmaleamylate derivatives is higher than that in citraconylate derivatives.[21] Thus, PAsp(DET–PMM) is expected to be more rapidly converted to the parent polycation PAsp(DET) in acidic endosomes compared with PAsp(DET–ACO), for facilitating the endosome disruption (Figure S1, Supporting Information). The successful synthesis of PEG–PAsp(DET–PMM) was confirmed from the size exclusion chromatogram (Figure S2, Supporting Information) and $^1$H NMR spectrum (Figure S3 and Table S1, Supporting Information).

The charge-conversion functionality of PEG–PAsp(DET–PMM) was compared with that of PEG–PAsp(DET–ACO) by determining the amount of amines generated from the CCP segments at pH 7.4 and 5.5 (Figure 2). Obviously, PEG–PAsp(DET–PMM) exerted higher conversion rate than PEG–PAsp(DET–ACO) over time at both pHs of 5.5 and 7.4, demonstrating more rapid hydrolysis of the PMM amide bonds. Also, the accelerated hydrolysis at the lower pH of 5.5 was demonstrated for both CCP segments. Nevertheless, the considerable increase in the conversion ratios even at pH 7.4 is likely to induce destabilization of hybrid micelles under extracellular neutral conditions. Thus, the stability of hybrid micelles in serum-containing medium was further examined as described below.

The newly synthesized PEG–CCP, PEG–PAsp(DET–PMM), was applied for the preparation of CaP hybrid micelles loaded with siRNA and then characterized by DLS. The obtained DLS (volume-weighted) histogram of siRNA-loaded hybrid micelles prepared with PEG–PAsp(DET–PMM) (PMM micelles) displays a hydrodynamic diameter of ≈70 nm (Figure S4, Supporting Information), associated with a narrow size distribution (polydispersity index = 0.1), similar to hybrid micelles prepared with PEG–PAsp(DET–ACO) (ACO micelles). Note that the micelle formation was not observed in the absence of calcium and phosphate ions under the similar condition because of the hydrophilic nature of PEG–CCPs. In sharp contrast, non-PEGylated CaP precipitates showed much larger size (≈1 μm) (data not shown). These results demonstrate that the block copolymers with PEG were essential for the sub-100 nm nanoparticle formation due to enhanced colloidal stability based on the PEG shell.

The carrier stability under cell culture conditions is a prerequisite for efficient cellular uptake of siRNA. In our previous study, ACO micelles were confirmed to stably entrap siRNA in 10% fetal bovine serum (FBS)-containing Dulbecco's modified Eagle's medium (DMEM) for a relatively short incubation time of 4 h.[17] Nevertheless, the stable entrapment of siRNA in the micelles for longer incubation time (e.g., 24 h) is crucial from the standpoint of systemic delivery. Thus, the stability of hybrid micelles in the DMEM containing 10% FBS was investigated over 24 h at 37 °C by fluorescence correlation spectroscopy.[17,23] By assuming the spherical shape of hybrid micelles,[17,18] the obtained diffusion coefficients of hybrid micelles incorporating Alexa647-siLuc were converted to the corresponding hydrodynamic diameters based on the Stokes-Einstein equation (Figure S5, Supporting Information), and then, normalized to the value of naked siRNA. Both hybrid micelles maintained their initial size during 24 h incubation, indicating the stable encapsulation of siRNA within the hybrid micelles in the serum-containing medium. These results strongly suggest that PEG–PAsp(DET–PMM) and PEG–PAsp(DET–ACO) should be stably bound to CaP core without hydrolysis of maleic acid amides in the serum-containing medium at pH 7.4.

Next, the cellular internalization behavior of hybrid micelles was examined by a flow cytometer. Luciferase-expressing human ovarian cancer (SKOV3-Luc) cells were incubated with Cy5-siLuc-loaded hybrid micelles for 6 and 24 h, followed by the flow cytometric analysis (Figure 3A and Figure S6, Supporting Information). The significant cellular uptake of Cy5-siLuc was confirmed for all three hybrid micelles, i.e., PMM micelles, ACO micelles,

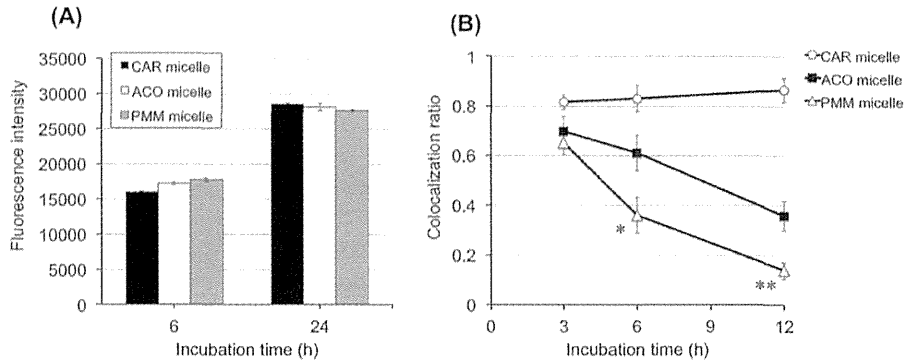


*Figure 3.* A) Cellular uptake efficiency of Cy5-siLuc delivered by hybrid micelles in SKOV3-Luc cells after 6 h incubation and 24 h incubation ($100 \times 10^{-9}$ M siRNA). Results are expressed as mean ± SEM ($n = 3$). (B) Time-dependent change in colocalization ratio of Alexa647-siLuc (red) with CellLight Late Endosomes-GFP (green) in SKOV3-Luc cells ($200 \times 10^{-9}$ M siRNA). The data are represented as mean ± SEM obtained from 14 cells ($^{*}p < 0.05$, $^{**}p < 0.01$).

and the micelles prepared with PEG–PAsp(DET–CAR) as a non-charge-conversion control polymer (nonCCP), in 6 h incubation. The uptake was further increased by prolonging the incubation time to 24 h. Importantly, almost the same cellular internalization profiles were observed among the three micelles, presumably because they have similar PEGylated shell structures. Next, the intracellular trafficking of hybrid micelles was investigated as a critical step following the cellular internalization. In particular, the colocalization of hybrid micelles (or the siRNA payload) with the late endosomes was focused to verify the endosome-escaping functionality of PEG–PAsp(DET–PMM) in comparison with PEG–PAsp(DET–ACO) and PEG–PAsp(DET–CAR). SKOV3-Luc cells were incubated with each hybrid micelle prepared with Alexa647-siLuc,

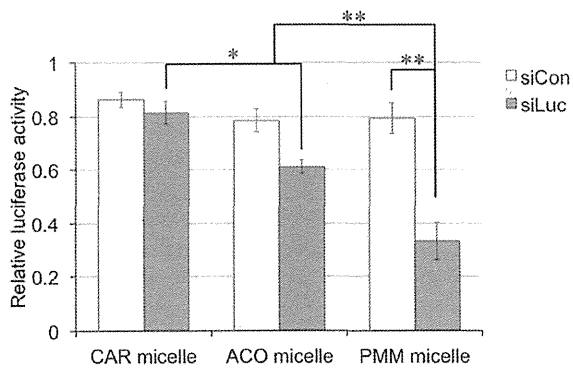


*Figure 4.* Luciferase gene silencing efficiency of CAR micelles, ACO micelles, and PMM micelles in SKOV3-Luc cells. The cells were incubated with each micelle incorporating siLuc (target sequence) or siCon (control sequence) at $50 \times 10^{-9}$ M siRNA for 48 h, followed by a conventional luciferase assay. The obtained luminescence intensities from cell lysates were normalized to that from non-treated control cells. Results are shown as mean ± SEM ($n = 6$, $^{*}p < 0.05$, $^{**}p < 0.01$).

and then, the transfection medium containing the hybrid micelles was exchanged with the fresh one without micelle samples, followed by additional incubation before confocal laser scanning microscope (CLSM) imaging. The intracellular Alexa647-siLuc was shown red and also the endosomal membrane was stained with CellLight Late Endosomes-GFP (green), thereby their colocalization points within the cells should be shown yellow in the merged CLSM images (Figure S7, Supporting Information). Then, the colocalization ratio of Alexa647-siLuc with the stained late endosomes at the designated time points was calculated by pixel counting for each hybrid micelle (Figure 3B), as described in Supporting Information. The CCP-integrated micelles, i.e., PMM and ACO micelles, showed time-dependent decreases in the colocalization ratio from 3 to 12 h, whereas the colocalization ratio of the nonCCP-integrated, CAR micelles was not significantly altered. This result strongly suggests the facilitated endosomal escape of Alexa647-siLuc by the CCPs integrated into the hybrid micelles. Further, the colocalization ratio of PMM micelles was significantly lower than that of ACO micelles, demonstrating stronger endosome-escaping functionality of the CCP integrated with PAsp(DET–PMM). On the contrary, the apparently high colocalization ratios of CAR micelles indicate that the hybrid micelles without CCPs could not effectively induce the endosome disruption under the tested condition. These results are consistent with the polymer design concept that more rapid conversion of CCPs to the endosome-disrupting polycation PAsp(DET) at an endosomal acidic pH of 5.5 should enable more efficient endosomal escape of hybrid micelles.

The gene silencing efficiency of hybrid micelles was determined to elucidate the effect of endosome-escaping functionality of CCPs on the ultimate biological activity of siRNA. The hybrid micelles prepared with a target sequence of siRNA (siLuc) or a control sequence (siCon)

were incubated with SKOV3-Luc cells at $50 \times 10^{-9}$ M siRNA for 48 h, followed by a luciferase assay of the cell lysates (Figure 4). The siLuc/CCP-loaded micelles (i.e., PMM and ACO micelles) achieved significantly lower luciferase activity compared to the siLuc/nonCCP-loaded micelles (i.e., CAR micelles), indicating the greater gene silencing efficiency of hybrid micelles equipped with CCPs. The PMM micelles revealed further improved efficiency in gene silencing compared to the ACO micelles. Considering the similar cellular internalization behaviors of the three hybrid micelles (Figure 3A), it is reasonable to conclude that the greater gene silencing efficiency of the PMM hybrid micelles is mainly due to their improved capability of translocating siRNA payloads from endosomal compartment to cytosol based on their prominent charge-conversion functionality (Figure 3B). It should be noted that the significant difference in relative luciferase activity was observed between siLuc-loaded and siCon-loaded micelles and also that the PMM micelles did not affect the viability of SKOV3-Luc cells under the same condition as the gene silencing assay (Figure S8, Supporting Information). These results confirm the sequence-specific gene silencing effect of siLuc-loaded hybrid micelles.

## 4. Conclusions

In this study, PEG–PAsp(DET–PMM) was synthesized by utilizing PMM amide, which was more sensitive to acid hydrolysis compared to the previously developed ACO amide. The obtained PEG–PAsp(DET–PMM) successfully formed siRNA-loaded hybrid micelles having the size of ≈70 nm. The PMM micelles were stable in the 10% FBS-containing medium at least for 24 h, leading to the efficient cellular uptake of siRNA in cultured SKOV3-Luc cells, similar to ACO micelles. Ultimately, the PMM micelles achieved the greater gene silencing activity in the cells, compared to ACO micelles, presumably due to the more efficient endosomal escape of the siRNA payload by PEG–PAsp(DET-PMM). These results demonstrate that the fine-tuning of endosome-disrupting polymers improves the delivery efficacy of siRNA nanocarriers for enhanced gene silencing activity.

## Supporting Information

Supporting Information is available from the Wiley Online Library or from the author.

Acknowledgements: This research was funded by JSPS through the "Funding Program for World-Leading Innovative R&D on Science and Technology (FIRST Program)", JST through Center of Innovation (COI) and Adaptable and Seamless Technology Transfer Program through Target-driven R&D (A-STEP), National Institute of Biomedical Innovation (NIBIO), and the Japanese Ministry of Health, Labour and Welfare through Grants-in-Aid for Scientific Research. Part of this work was conducted in the Research Hub for Advanced Nano Characterization, The University of Tokyo, supported by the Ministry of Education, Culture, Sports, Science and Technology (MEXT), Japan. The authors are grateful to A. Miyoshi for their assistance with experiments.

Received: January 24, 2014; Revised: March 3, 2014; Published online: April 8, 2014; DOI: 10.1002/marc.201400049

Keywords: calcium phosphate; poly(ethylene glycol); polymeric micelles; pH-responsive polymer; siRNA

[1] J. C. Burnett, J. J. Rossi, *Chem. Biol.* **2012**, *19*, 60.
[2] J. Gruenberg, F. G. van der Goot, *Nat. Rev. Mol. Cell Biol.* **2006**, *7*, 495.
[3] E. Wagner, *Acc. Chem. Res.* **2012**, *45*, 1005.
[4] O. Boussif, F. Lezoualc'h, M. A. Zanta, M. D. Mergny, D. Scherman, B. Demeneix, J. P. Behr, *Proc. Natl. Acad. Sci. USA* **1995**, *92*, 7297.
[5] Z. U. Rehman, D. Hoekstra, I. S. Zuhorn, *ACS Nano* **2013**, *7*, 3767.
[6] T. Bieber, W. Meissner, S. Kostin, A. Niemann, H. P. Elsasser, *J. Controlled Release* **2002**, *82*, 441.
[7] C. W. Evans, M. Fitzgerald, T. D. Clemons, M. J. House, B. S. Padman, J. A. Shaw, M. Saunders, A. R. Harvey, B. Zdyrko, I. Luzinov, G. A. Silva, S. A. Dunlop, K. S. Iyer, *ACS Nano* **2011**, *5*, 8640.
[8] S. M. Moghimi, P. Symonds, J. C. Murray, A. C. Hunter, G. Debska, A. Szewczyk, *Mol. Ther.* **2005**, *11*, 990.
[9] G. Grandinetti, N. P. Ingle, T. M. Reineke, *Mol. Pharm.* **2011**, *8*, 1709.
[10] N. Kanayama, S. Fukushima, N. Nishiyama, K. Itaka, W. D. Jang, K. Miyata, Y. Yamasaki, U. I. Chung, K. Kataoka, *ChemMedChem* **2006**, *1*, 439.
[11] K. Miyata, N. Nishiyama, K. Kataoka, *Chem. Soc. Rev.* **2012**, *41*, 2562.
[12] K. Masago, K. Itaka, N. Nishiyama, U.-I. Chung, K. Kataoka, *Biomaterials* **2007**, *28*, 5169.
[13] K. Miyata, M. Oba, M. Nakanishi, S. Fukushima, Y. Yamasaki, H. Koyama, N. Nishiyama, K. Kataoka, *J. Am. Chem. Soc.* **2008**, *130*, 16287.
[14] H. Uchida, K. Miyata, M. Oba, T. Ishii, T. Suma, K. Itaka, N. Nishiyama, K. Kataoka, *J. Am. Chem. Soc.* **2011**, *133*, 15524.
[15] Y. Lee, K. Miyata, M. Oba, T. Ishii, S. Fukushima, M. Han, H. Koyama, N. Nishiyama, K. Kataoka, *Angew. Chem. Int. Ed.* **2008**, *47*, 5163.
[16] F. Pittella, M. Zhang, Y. Lee, H. J. Kim, T. Tockary, K. Osada, T. Ishii, K. Miyata, N. Nishiyama, K. Kataoka, *Biomaterials* **2011**, *32*, 3106.
[17] F. Pittella, K. Miyata, Y. Maeda, T. Suma, S. Watanabe, Q. Chen, R. J. Christie, K. Osada, N. Nishiyama, K. Kataoka, *J. Controlled Release* **2012**, *161*, 868.
[18] F. Pittella, H. Cabral, Y. Maeda, P. Mi, S. Watanabe, H. Takemoto, H. J. Kim, N. Nishiyama, K. Miyata, K. Kataoka, *J. Controlled Release***2014**, *178*, 18.
[19] A. Tabaković, M. Kester, J. H. Adair, *WIREs Nanomed. Nanobiotechnol.* **2012**, *4*, 96.
[20] W. A. Blattler, B. S. Kuenzi, J. M. Lambert, P. D. Senter, *Biochemistry* **1985**, *24*, 1517.
[21] D. B. Rozema, K. Ekena, D. L. Lewis, A. G. Loomis, J. A. Wolff, *Bioconjugate Chem.* **2003**, *14*, 51.
[22] R. L. Juliano, X. Ming, O. Nakagawa, *Bioconjugate Chem.* **2012**, *23*, 147.
[23] K. Buyens, M. Meyer, E. Wagner, J. Demeester, S. C. De Smedt, N. N. Sanders, *J. Controlled Release* **2010**, *141*, 38.

Biomaterials 35 (2014) 7887–7895

Contents lists available at ScienceDirect

Biomaterials

journal homepage: www.elsevier.com/locate/biomaterials

# Actively-targeted polyion complex micelles stabilized by cholesterol and disulfide cross-linking for systemic delivery of siRNA to solid tumors

Yusuke Oe [a], R. James Christie [a], Mitsuru Naito [b], Stewart A. Low [b], Shigeto Fukushima [b], Kazuko Toh [a], Yutaka Miura [a], Yu Matsumoto [a], Nobuhiro Nishiyama [a, c], Kanjiro Miyata [a, **], Kazunori Kataoka [a, b, d, e, *]

[a] Center for Disease Biology and Integrative Medicine, Graduate School of Medicine, The University of Tokyo, 7-3-1 Hongo, Bunkyo-ku, Tokyo 113-0033, Japan
[b] Department of Materials Engineering, Graduate School of Engineering, The University of Tokyo, 7-3-1 Hongo, Bunkyo-ku, Tokyo 113-8656, Japan
[c] Polymer Chemistry Division, Chemical Resources Laboratory, Tokyo Institute of Technology, R1-11, 4259 Nagatsuta, Midori-ku, Yokohama 226-8503, Japan
[d] Department of Bioengineering, Graduate School of Engineering, The University of Tokyo, 7-3-1 Hongo, Bunkyo-ku, Tokyo 113-8656, Japan
[e] Center for NanoBio Integration, The University of Tokyo, 7-3-1 Hongo, Bunkyo-ku, Tokyo 113-8656, Japan

ARTICLE INFO

*Article history:*
Received 13 May 2014
Accepted 16 May 2014
Available online 13 June 2014

*Keywords:*
siRNA delivery
Polyion complex micelle
Active targeting
Cyclic RGD peptide
Cholesterol modified siRNA

ABSTRACT

For small interfering RNA (siRNA)-based cancer therapies, we report an actively-targeted and stabilized polyion complex micelle designed to improve tumor accumulation and cancer cell uptake of siRNA following systemic administration. Improvement in micelle stability was achieved using two stabilization mechanisms; covalent disulfide cross-linking and non-covalent hydrophobic interactions. The polymer component was designed to provide disulfide cross-linking and cancer cell-targeting cyclic RGD peptide ligands, while cholesterol-modified siRNA (Chol-siRNA) provided additional hydrophobic stabilization to the micelle structure. Dynamic light scattering confirmed formation of nano-sized disulfide cross-linked micelles (<50 nm in diameter) with a narrow size distribution. Improved stability of Chol-siRNA-loaded micelles (Chol-siRNA micelles) was demonstrated by resistance to both the dilution in serum-containing medium and counter polyion exchange with dextran sulfate, compared to control micelles prepared with Chol-free siRNA (Chol-free micelles). Improved stability resulted in prolonged blood circulation time of Chol-siRNA micelles compared to Chol-free micelles. Furthermore, introduction of cRGD ligands onto Chol-siRNA micelles significantly facilitated accumulation of siRNA in a subcutaneous cervical cancer model following systemic administration. Ultimately, systemically administered cRGD/Chol-siRNA micelles exhibited significant gene silencing activity in the tumor, presumably due to their active targeting ability combined with the enhanced stability through both hydrophobic interactions of cholesterol and disulfide cross-linking.



## 1. Introduction

Small interfering RNA (siRNA) inhibits expression of genes by a sequence-specific gene silencing effect, known as RNA interference (RNAi) [1–3]. This property has generated much interest for development of siRNA drugs that inhibit production of proteins associated with disease. However, low bioavailability of siRNA has hampered its translation into clinical use. Efforts to improve the efficacy of siRNA drugs have led to development of many types of siRNA-loaded nanoparticles to overcome biological hurdles associated with siRNA delivery, e.g., enzymatic degradation, accumulation in non-target organs/tissues and inefficient cellular uptake [4–6]. In particular, the ability to target specific cells has proven to be highly effective for enhanced accumulation of nanoparticles in solid tumors through systemic administration and has also been

* Corresponding author. Center for Disease Biology and Integrative Medicine, Graduate School of Medicine, The University of Tokyo, 7-3-1 Hongo, Bunkyo-ku, Tokyo 113-0033, Japan. Tel.: +81 3 5841 7138; fax: +81 3 5841 7139.
** Corresponding author. Tel.: +81 3 5841 1701; fax: +81 3 5841 7139.
*E-mail addresses:* miyata@bmw.t.u-tokyo.ac.jp (K. Miyata), kataoka@bmw.t.u-tokyo.ac.jp (K. Kataoka).

http://dx.doi.org/10.1016/j.biomaterials.2014.05.041
0142-9612/

shown to facilitate cellular/subcellular delivery of siRNA [7–16]. Thus, a variety of ligand molecules that bind to specific receptors on cancer cells have been installed on the surface of nanoparticles [7–16]. In order to take full advantage of such targeting ligands, however, maintaining the nanoparticle structure in circulation is essential; targeting ligands can cooperatively function when distributed on the nanoparticle surface, allowing for avidity through multisite binding [13,15,17,18]. Therefore, a highly effective siRNA delivery system should result from incorporating cellular surface-targeting ability to a nanoparticle platform resistant to destabilization (or dissociation), thus maximizing the ligand binding effect.

A promising platform for systemic siRNA delivery into solid tumors is the polyion complex (PIC) micelle, constructed with block copolymers of poly(ethylene glycol) (PEG) and a polycation as an siRNA binding segment [13,16,19–22]. Charge neutralization between siRNA and the polycationic segment of the block copolymer in aqueous solution enables formation of PIC micelles, in which the siRNA-loaded PIC core is surrounded by a nonionic and hydrophilic PEG shell. This core–shell structure results in enhanced colloidal stability and reduced nonspecific interactions with charged biomacromolecules. To further increase micelle stability for *in vivo* delivery, several stabilizing approaches via hydrophobic interactions [16,23] or disulfide cross-links [13,24–26] have been investigated so far. Disulfide cross-links are noteworthy as they impart reversible stability to the micelle core upon cleavage (reduction) in the cell interior in response to the increased glutathione concentration, which is 100–1000 times higher than that in the cell exterior [27,28]. Reversible micelle stability is an important feature for nucleic acid delivery vehicles, since siRNA release into the cytoplasm is required to access the RNAi pathway.

Meanwhile, our previous studies revealed that siRNA micelles could be disrupted even with disulfide cross-linking in the core, leading to undesirable release of siRNA payloads [26]. These results suggest that the cross-linking within the micelle core may be highly localized, incapable of stabilizing the whole core structure. Thus, an additional stabilizing mechanism may further reinforce the cross-linked siRNA micelle structure, leading to longer blood circulation and enhanced tumor accumulation. Herein, cholesterol-conjugated siRNA (Chol-siRNA) [29] was utilized to stabilize micelle core structures in addition to disulfide cross-linking. Hydrophobized siRNAs are expected to suppress micelle disruption and subsequent leakage of siRNA due to hydrophobic associations of cholesterol groups [16,30]. Therefore, the combined use of a thiolated block copolymer and Chol-siRNA creates a stable, yet reversible, platform for improved systemic siRNA delivery.

In this work, we employed a functional block copolymer comprising PEG segment installed with cyclo-Arg-Gly-Asp (cRGD) peptide as the tumor-targeting hydrophilic block [13,16,31] and poly(L-lysine) (PLL) segment modified with dithiobispropionimidate (DTBP) as the cationic block [26]. DTBP modification was chosen for generating a single and stable side chain structure comprising an amidine and thiol functionality, making polyionic pairs/hydrogen bonds with siRNA phosphates in addition to disulfide cross-linking [26]. After examining the contribution of Chol-siRNA to micelle stability, the targeting ability of cRGD ligand was verified utilizing a luciferase-expressing cervical cancer (HeLa-Luc) cell line. Finally, the *in vivo* siRNA delivery efficacy of the actively-targeted/stabilized micelles was evaluated by luciferase gene silencing activity in the murine subcutaneous tumors after systemic administration, demonstrating strong potential for tumor-targeted systemic siRNA delivery.

## 2. Materials and methods

### 2.1. Materials

$D_2O$ (99.9%), tetramethylsilane (TMS, 99.5%), boric acid, trizma base and Dulbecco's modified Eagle's medium (DMEM) were purchased from Sigma Aldrich (St. Louis, MO) and used without further purification. Dithiothreitol (DTT, molecular biology grade DNase and RNase free), ethylenediamine tetraacetic acid disodium salt dihydrate (EDTA, 99.5%) and ethidium bromide solution were supplied by Wako Pure Chemical Industries (Osaka, Japan). Dimethyl-3,3′-dithiobispropionimidate/2HCl (DTBP/HCl) and slide-a-lyzer dialysis cassettes (MWCO 3500 Da) were purchased from Thermo Scientific (Rockford, IL). Sterile HEPES (1 M, pH 7.3) was purchased from Amresco (Solon, OH). Agarose L03 TAKARA was purchased from Takara Bio Inc (Shiga, Japan) and used for gel electrophoresis. Cell Counting Kit 8 (CCK-8) was purchased from Dojindo Laboratories (Kumamoto, Japan). Cyclo-[RGDfK(C-∑-Acp)] (cRGD) peptide was synthesized by Peptide Institute Inc. (Osaka, Japan). A series of siRNAs were synthesized by Hokkaido System Science Co., Ltd. (Hokkaido, Japan) and their sequences were as follows; (1) firefly GL3 luciferase (siLuc): 5′-CUU ACG CUG AGU ACU UCG AdTdT-3′ (sense), 5′-UCG AAG UAC UCA GCG UAA GdTdT-3′ (antisense); (2) control scramble sequence (siScr): 5′-UUC UCC GAA CGU GUC ACG UdTdT-3′ (sense), 5′-ACG UGA CAC GUU CGG AGA AdTdT-3′ (antisense). Cy5 dye and Chol moiety were introduced to the 5′-end of the antisense strand and the sense strand, respectively.

### 2.2. Synthesis of cyclic RGD peptide-poly(ethylene glycol)-block-poly(L-lysine) (cRGD-PEG-PLL)

cRGD-PEG-PLL and methoxy-PEG-PLL (termed PEG-PLL) block copolymers (molecular weight (MW) of PEG: 12,000 Da; degree of polymerization (DP) of PLL segment: approximately 45) were synthesized as previously described [13,19,31]. The cRGD peptide was introduced to the PEG terminus of acetal-PEG-PLL through the thiazolidine ring formation between the N-terminal cysteine of cRGD and the aldehyde group generated in acetal-PEG-PLL after incubation at acidic pH [31]. The obtained polymer (yield: 112 mg, 86%) was characterized at 22 °C by $^1$H NMR (JEOL ECS-400, JEOL, Tokyo, Japan). The amount of cRGD conjugated to the polymer was estimated from $^1$H NMR spectrum based on the peak intensity ratio of phenyl protons in cRGD peptide (D-Phe, $\delta$ = 7.2–7.4 ppm) to ethylene protons in PEG ($-CH_2CH_2-$, $\delta$ = 3.6–3.8 ppm) (Fig. S1). The cRGD introduction rate was calculated to be approximately 70%.

### 2.3. Synthesis of cyclic RGD peptide-poly(ethylene glycol)-block-poly(L-lysine modified with 1-(3-mercaptopropyl)amidine) (cRGD-PEG-PLL(MPA))

cRGD-PEG-PLL(MPA) was synthesized by introducing MPA moieties into the lysine primary amines in cRGD-PEG-PLL using DTBP, as shown in Scheme 1 [26]. Briefly, cRGD-PEG-PLL (50 mg, 0.1 mmol amines) was dissolved in 100 mM borate buffer (pH 9.0) (10 mL), followed by the addition of DTBP/HCl (69 mg, 0.2 mmol). The reaction solution was stirred at 25 °C for 45 min and then dialyzed (MWCO 3500 Da) against 10 mM PBS (pH 6.0) for 2 h and distilled water for 2 h. The dialyzed solution was lyophilized after filtration (yield: 53.9 mg, 80%). The substitution degree of MPA groups in the obtained polymer was determined from the $^1$H NMR spectrum based on the peak intensity ratio of β, γ and δ methylene protons in PLL side chains ($-(CH_2)_3-$, $\delta$ = 1.3–1.9 ppm) to mercaptoethyl protons in MPA moieties ($HS-(CH_2)_2-$, $\delta$ = 2.7–2.9 ppm) (Fig. 1), demonstrating quantitative introduction (>97%). In a similar manner, PEG-PLL(MPA) without cRGD peptide was synthesized by the reaction of PEG-PLL with DTBP (Scheme 1). For PEG-PLL(MPA), PEG-PLL (300 mg, 0.71 mmol amines) and DTBP/HCl (439 mg, 1.4 mol) were used (yield: 299 mg, 73%). Quantitative introduction of MPA group (>99%) was also confirmed by $^1$H NMR analysis (Fig. S2).

### 2.4. Polyionic complexation of block copolymers with siRNA

cRGD-PEG-PLL(MPA) (or PEG-PLL(MPA)) block copolymer was dissolved in 10 mM HEPES buffer (pH 7.4) and incubated with 100 mM DTT at 25 °C for 15 min for disulfide reduction. The reduced polymer solution was mixed with siRNA dissolved in the same buffer (15 μM siRNA) at different molar charge ratios of the block copolymer to siRNA, i.e., amidines and primary amines in the block copolymer/phosphates in siRNA. To proceed disulfide cross-linking in the PIC core, PIC solutions (10 μM siRNA) were dialyzed (MWCO 3500 Da) against 5 mM HEPES (pH 7.4) containing 0.5% (v/v) DMSO for 2 days and 5 mM HEPES (pH 7.4) for 2 days. Dialyzed PIC solutions were filtered (0.22 μm) before characterization. In a similar manner, control PICs without Chol moieties were also prepared with PEG-PLL(MPA) and siRNA. For *in vivo* experiments, micelle solutions were dispersed in 5 mM HEPES (pH 7.4) and made isotonic by addition of 1.5 M NaCl to a final concentration of 150 mM.

### 2.5. Static and dynamic light scattering (SLS and DLS) analyses

SLS and DLS measurements were performed with a ZetaSizer Nano ZS instrument (Malvern Instruments Ltd., Worcestershire, UK) equipped with a He–Ne laser ($\lambda$ = 633 nm) as the incident beam. All measurements were made at 25 °C and a detection angle of 173°. PIC samples (10 μM siRNA, 18 μL) dispersed in 5 mM HEPES buffer (pH 7.4) were loaded into a low-volume cuvette (Zen 2112) for each analysis.

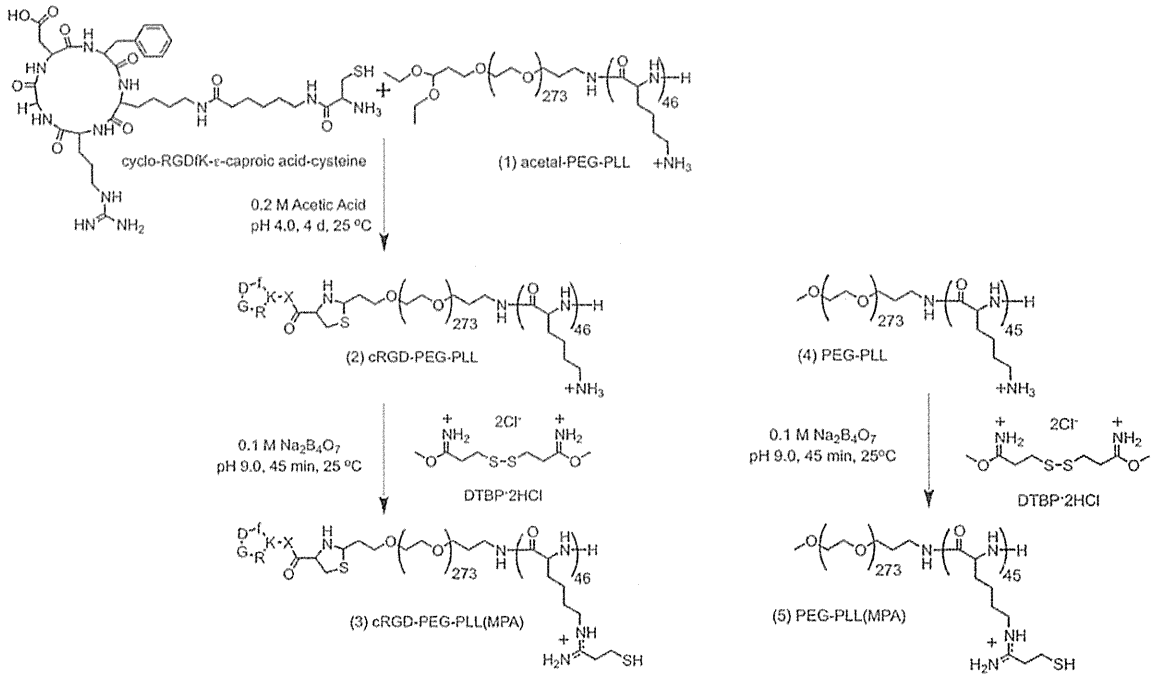


**Scheme 1.** Synthesis schemes of cRGD-PEG-PLL(MPA) and PEG-PLL(MPA).

Scattered light intensity (SLI) was measured to monitor micelle formation, using a constant attenuator setting in the instrument. Cumulant size, polydispersity index (PDI), and size distribution (intensity-weighted) histogram were calculated based on the autocorrelation function of samples, with automated attenuator adjustment and multiple scans (typically 12–30 scans) for optimal accuracy.

### 2.6. Fluorescence correlation spectroscopy (FCS) measurement

Diffusion time of fluorescently-labeled micelles (or naked siRNA) was measured by FCS using samples prepared with Cy5-labeled siRNA (Cy5-siRNA). Samples containing 10 μM Cy5-siRNA were diluted with PBS containing 10% FBS, followed by 1 h incubation. Then, the samples were placed into an 8-well Lab-Tek chambered borosilicate cover-glass (Nalge Nunc International, Rochester, NY) and measured with a combination system of ConfoCor3 module and LSM510 equipped C-Apochromat 40×, N.A. 1.2 water immersion objective (Carl Zeiss, Oberkochen, Germany) (sampling time: 10 s, repeating time: 10). A He–Ne laser (633 nm) was used for excitation of Cy5-siRNA and emission was filtered through the corresponding band-pass filter. The measured autocorrelation curves were fitted with the Zeiss Confocor3 software package to obtain the corresponding diffusion time. The obtained diffusion time was converted to the corresponding hydrodynamic diameter by the Stokes-Einstein equation.

### 2.7. Gel electrophoresis

Agarose gel was prepared by adding agarose (0.7 g) to a TBE buffer (70 mL) prepared with trizma base (10.8 g), boric acid (5.5 g) and EDTA/2Na (74 mg) in pure water (1 L). The mixture was heated to dissolve the agarose powder and then allowed to cool down before adding ethidium bromide (1 μL). Micelle solutions (2 μL) with or without DTT (200 mM DTT) were mixed with dextran sulfate solutions (2 μL). The concentrations of dextran sulfate groups were set at 0, 1.0, 1.5, 2.0 and 3.0 times equivalent to the siRNA phosphates. After incubation for 2 h at 25 °C, each sample was loaded on the gel and electrophoresed (100 V, 30 min) in TBE running buffer. After electrophoresis, gel images were captured by a Typhoon 9410 instrument equipped with a 532 nm laser. Also, micelle samples were subjected to the electrophoresis (50 V, 30 min) after incubation with different amounts of anionic lipid, DOPS (1,2-dioleoyl-sn-glycero-3-phospho-L-serine sodium salt), for 8 h at 25 °C.

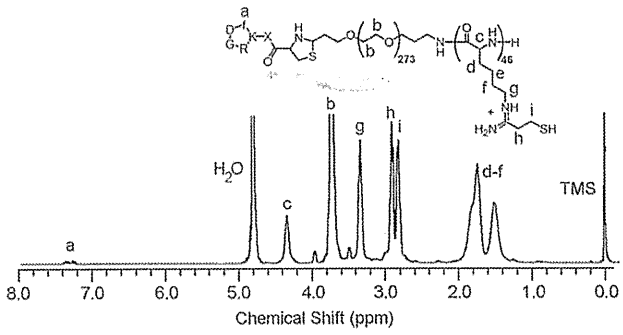


**Fig. 1.** $^1H$ NMR spectrum of cRGD-PEG-PLL(MPA), recorded in $D_2O$ (10 mg/mL) at 25 °C.

### 2.8. Cellular uptake

Luciferase-expressing human cervical cancer cells, HeLa-Luc (Caliper LifeScience, Hopkinton, MA), were seeded into 6-well plates (100,000 cells/well) and incubated in DMEM containing 10% fetal bovine serum (FBS) (Dainippon Sumitomo Pharma Co. Osaka, Japan) (1.5 mL) for 24 h. The culture media were then exchanged with fresh media containing micelle samples prepared with Cy5-siRNA (siRNA concentration: 333 nM). Cells were incubated in the presence of micelles for 75 min at 37 °C and then further incubated in the absence of micelles for 8 h after medium exchange. The cells were harvested by trypsinization, followed by flow cytometric analyses using a BD LSR II instrument (BD Biosciences, San Jose, CA) and BD FACS Diva software (BD Biosciences).

### 2.9. In vitro luciferase assay

HeLa-Luc cells were seeded in 35 mm dishes (25,000 cells/dish) and incubated in DMEM containing 10% FBS (2 mL) for 24 h. Then, the culture media were exchanged with fresh media (2 mL) containing 100 μM luciferin (Summit Pharmaceutical International, Tokyo, Japan) and micelle samples (200 nM siRNA). For each analysis, control samples were prepared by treating cells with 5 mM HEPES buffer (pH 7.4). Samples were placed into a Kronos real-time photon countable incubator (ATTO Corp., Tokyo, Japan) at 37 °C and 5% $CO_2$ and the luminescence intensity (counts) was measured periodically over 50 h. Relative luminescence intensity was determined by normalizing the average luminescence intensity of treated samples ($n = 4$) to the average luminescence intensity of control samples ($n = 4$).

### 2.10. Cytotoxicity assay

HeLa-Luc cells were seeded in 24-well plates (20,000 cells/well) and incubated in DMEM containing 10% FBS (0.5 mL) for 24 h. Thereafter, the culture media were replaced with fresh media containing micelle samples at varying siRNA concentrations and cells were further incubated for 48 h. Then, CCK-8 solution (1 μL/10 μL medium) was added and samples were further incubated at 37 °C for 1 h. Cell viability was determined from the absorbance of extracellular media at 450 nm,

which was measured using a BIO-RAD 680 microplate reader (Bio-Rad, CA). All data are expressed relative to untreated control cells ($n = 6$).

### 2.11. Blood circulation behavior

All animal experimental procedures were performed in accordance with the policies of the Animal Ethics Committee of The University of Tokyo. The blood circulation property of siRNA-loaded micelles was determined by IVRT-CLSM observation of live mice (BALB/c nude, female, 8 weeks old) (Charles River laboratories, Tokyo, Japan) using a Nikon A1R CLSM system attached to an upright ECLIPSE FN1 (Nikon Corp., Tokyo, Japan) equipped with a 20×, 640 nm diode laser, and a band-pass emission filter of 700/75 nm, as previously described [32]. The mice were anesthetized with 2–3% isoflurane (Abbott Japan Co., Ltd., Tokyo, Japan) using a Univenter 400 anesthesia unit (Univentor Ltd., Zejtun, Malta) and placed onto the temperature-controlled microscope stage. Blood vessels in the ear-lobe dermis were observed after tail vein injection of micelles prepared with Cy5-siRNA (3.6 nmol Cy5-siRNA/mouse, $n = 3$), as they were clearly observed without surgery (thus non-invasive) and were unaffected by the cardiac beat (thus steadily observed). The obtained images were analyzed by selecting regions of interest (ROIs) within blood vessels for determining the average fluorescence intensity at each time point. To produce blood circulation profiles shown in Fig. 5A, the vein fluorescence intensities were expressed as a relative value to the highest (1.0) and the lowest (0) obtained through the observation. In addition, the time point for the highest fluorescence intensity was defined as $t = 0$.

### 2.12. Tumor accumulation

HeLa-Luc cells ($2.6 \times 10^6$ cells) were injected under the skin of mice for preparation of donor tumors. After 2 weeks, the donor tumors were excised and cut into pieces, then transplanted under the skin of host mice. After 8 days, the subcutaneous tumor-bearing mice were subjected to tail vein injection of micelles prepared with Cy5-siRNA (1.8 nmol Cy5-siRNA/mouse, $n = 4–5$). After 4 h, they were sacrificed, and tumors (and major organs) were excised, followed by fluorescence quantification using an IVIS instrument equipped with Living Image software. Total photon counts were normalized to the illumination time and the sample area as follows: fluorescence intensity = total photons/[illumination time (s) × area ($cm^2$)]. Further normalization was performed by dividing the fluorescence intensity from the tumors treated with RGD-free controls.

### 2.13. In vivo luciferase assay

Subcutaneous HeLa-Luc tumor models were prepared by *in vivo* passage of tumor fragments, as described in the former section. After 8 days, the tumor-bearing mice were subjected to the tail vein injection of micelle samples (1.8 nmol siRNA/mouse/injection, $n = 5$) at 48 h, 38 h and 24 h before measurement. A luciferin solution (50 mM, 200 μL) was injected intraperitoneally 25 min prior to measurement to obtain the stable luminescence intensity from tumors. The luminescence intensity (counts) was recorded using an IVIS instrument under the same condition for each image (acquisition time: 5 s, binning: small, f/stop: 1, and field of view: D). Tumor volumes were determined by manual measurement with a caliper and calculated using the following equation: volume = $ab^2/2$, where $a$ is the long axis and $b$ is the short axis measured. The luminescence intensity obtained from sample-treated tumors was normalized to the tumor volume and further to that from buffer-treated control tumors: relative luminescence intensity = total photons of sample/sample-treated tumor volume ($cm^3$)/total photons of buffer control/control-treated tumor volume ($cm^3$).

### 2.14. Data analysis

The experimental data were analyzed by Student's $t$-test. $p < 0.05$ was considered statistically significant.

## 3. Results and discussion

### 3.1. Synthesis of block copolymers and their characterizations

In order to create actively-targeted and stabilized PIC micelles, a functional block copolymer was synthesized to comprise a targeting ligand, cationic charges, and free thiol groups (Scheme 1). The cRGD peptide was utilized as the ligand for tumor targeting through specific binding to $\alpha_v\beta_3$ and $\alpha_v\beta_5$ integrins, which are overexpressed on various cancer cells [33,34]. Also, DTBP was selected as the thiolation reagent because a cationic amidine group is concurrently introduced following reaction with lysine amines, preserving the polymer ability to form ion pairs with siRNA phosphates [26]. First, the cRGD peptide was conjugated to acetal-PEG-PLL by thiazolidine ring formation between the aldehyde generated on the PEG terminus at low pH and the N-terminal cysteine residue contained on the cRGD peptide [31]. Next, cRGD-PEG-PLL (or PEG-PLL as a non-targeted control) was reacted with DTBP under basic conditions to generate cRGD-PEG-PLL(MPA) (or PEG-PLL(MPA)) bearing the desired amidine and thiol functionalities in PLL side chains. Successful introduction of cRGD (71%) and MPA modification of amines (97%) was confirmed by $^1$H NMR analysis of the cRGD-PEG-PLL(MPA) reaction product (Fig. 1). Similarly, quantitative reaction of DTBP with lysine amines in PEG-PLL lacking cRGD (>99%) was also confirmed (Fig. S2).

### 3.2. Preparation and characterization of Chol-siRNA micelles

Micelle formation behavior with Chol-siRNA was investigated in terms of SLI, size and PDI by light scattering measurements (SLS and DLS). SLI values were utilized for confirming whether i) the signal intensity (or S/N ratio) of samples was suitable for fitting and ii) the polymer/siRNA mixtures formed multimolecular assemblies (i.e. micelles) prior to fitting. The size and the PDI were then determined by appropriate fitting. PEG-PLL(MPA) was mixed with Chol-siRNA or Chol-free siRNA as a control at varying residual molar charge ratios of the block copolymer to siRNA (+:− ratio). SLI values observed for polymer/Chol-siRNA mixture increased sharply in +:− ratios from 0 to 1.2 (Fig. 2A), similar to those for Chol-free siRNA mixture, indicating formation of PIC micelles due to the charge-neutralization between the polymer and siRNA. At

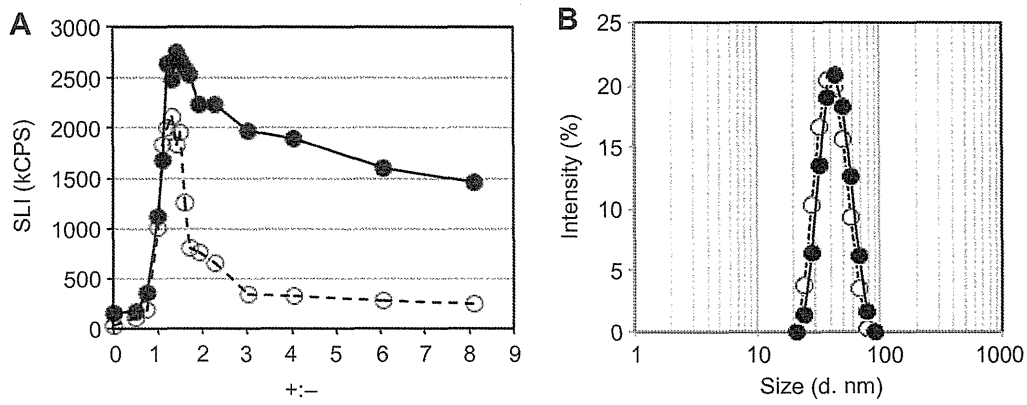


**Fig. 2.** Light scattering behavior of PEG-PLL(MPA) polymer and siRNA mixtures in 10 mM HEPES buffer (pH 7.4) at 25 °C. Open circles: Chol-free siRNA, closed circles: Chol-siRNA. A) SLI of mixtures at different +:− ratios. B) Intensity-weighted histograms of mixtures at +:− = 1.4.

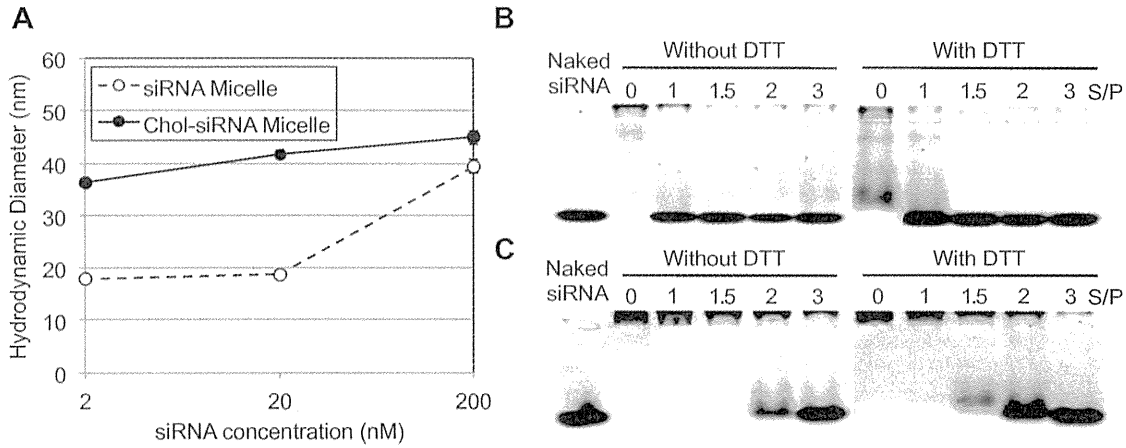


**Fig. 3.** Micelle stability assays. A) Change in size of Chol-free/Cy5-siRNA micelles and Chol/Cy5-siRNA micelles associated with dilution in 10% FBS-containing PBS. The diffusion time was measured by FCS and then the hydrodynamic diameter was calculated from the diffusion time (or diffusion coefficient) by the Stokes-Einstein equation. Each micelle was incubated for 1 h before measurements. Data represent the average value ± standard deviation (sampling time = 10 s, repetition time = 10). B and C) Agarose gel electrophoresis of siRNA micelles prepared with B) Chol-free siRNA and C) Chol-siRNA (0.3 μg) incubated with different concentrations of dextran sulfate under 0 or 100 mM DTT for 2 h. S/P ratio was defined as the molar ratio of sulfate groups in dextran sulfate to phosphate groups in siRNA.

+:− = 1.4, Chol-siRNA micelles were 43 ± 2 nm ($n = 3$) in cumulant diameter, and exhibited the lowest level of PDI (Fig. S3) as well as the highest SLI in the charge ratios tested. This slightly shifted +:− ratio from the charge-stoichiometric point is presumably due to the fact that complete ion-pair formation within PICs can be sterically hindered in block copolymers [26,35]. The intensity-weighted histograms at this mixing ratio clearly show the similar size distributions between Chol-siRNA and Chol-free micelles (Fig. 2B). These results confirm that the Chol moiety did not alter the micelle formation behavior between PEG-PLL(MPA) and siRNA at +:− <1.4. Note that a remarkable difference was observed between the two micelle formulations in their SLI values at +:− >1.4. The Chol-free siRNA mixture showed a drastic decrease in SLI, possibly due to the binding of a charge-excess amount of block copolymers to siRNA, generating electrostatic repulsion between PICs, and thus impeding their self-assemble into micelle structures [26]. In contrast, the Chol-siRNA mixture greatly resisted such decrease in SLI, indicating a stronger association force of Chol-siRNA PICs that can overcome electrostatic repulsion [30]. Meanwhile, the effect of MPA moieties in PEG-PLL(MPA) was additionally examined on the polyion complexation with Chol-siRNA by comparing with non-thiolated PEG-PLL. The PEG-PLL/Chol-siRNA mixtures showed the PDI of >0.18 in the tested mixing ratios from 0 to 4 (Fig. S3). These results demonstrate the crucial role of MPA moieties for the uniform micelle formation between Chol-siRNA and PEG-PLL(MPA); a possible explanation for the role of MPA moiety is that a higher degree of MPA moiety, i.e., thiol and guanidino groups, in the polycationic side chain could allow stronger intermolecular interactions with each other and/or siRNA through hydrogen bonding, dipole–dipole interactions, or Van der Waals force,

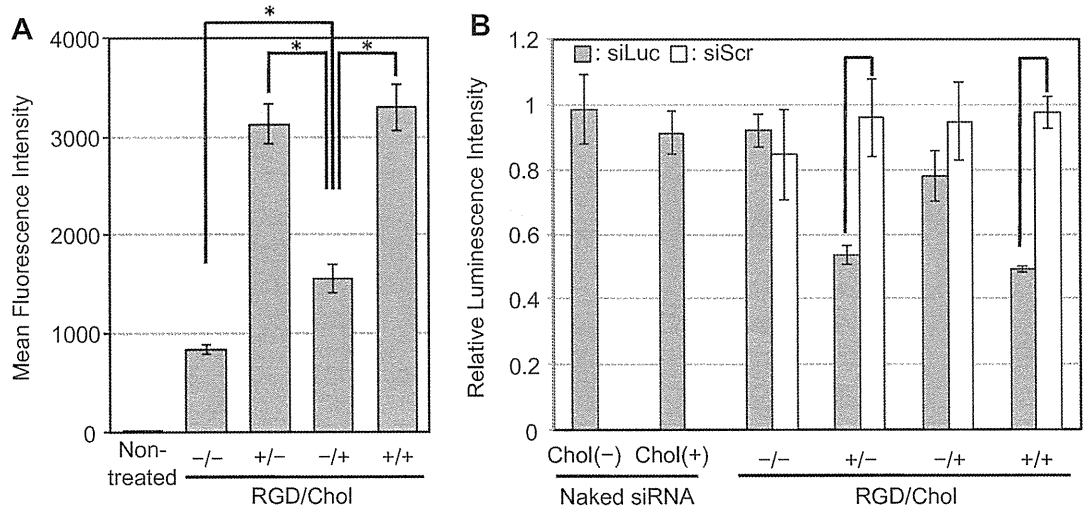


**Fig. 4.** A) Cellular uptake of Cy5-siRNA micelles in cultured HeLa-Luc cells, evaluated by flow cytometry. Cells were incubated with micelles for 75 min before medium change, and then further incubated for 8 h at 37 °C. Data represent the average value ± standard deviation ($n = 4$, *: $p < 0.05$). B) Gene silencing activity of naked siRNAs and siRNA micelles at 200 nM siRNA in cultured HeLa-Luc cells. Luminescence intensity was measured after 50 h incubation with siRNA samples and normalized to the value of nontreated control cells. Data represent the average value ± standard deviation ($n = 4$, *: $p < 0.05$).

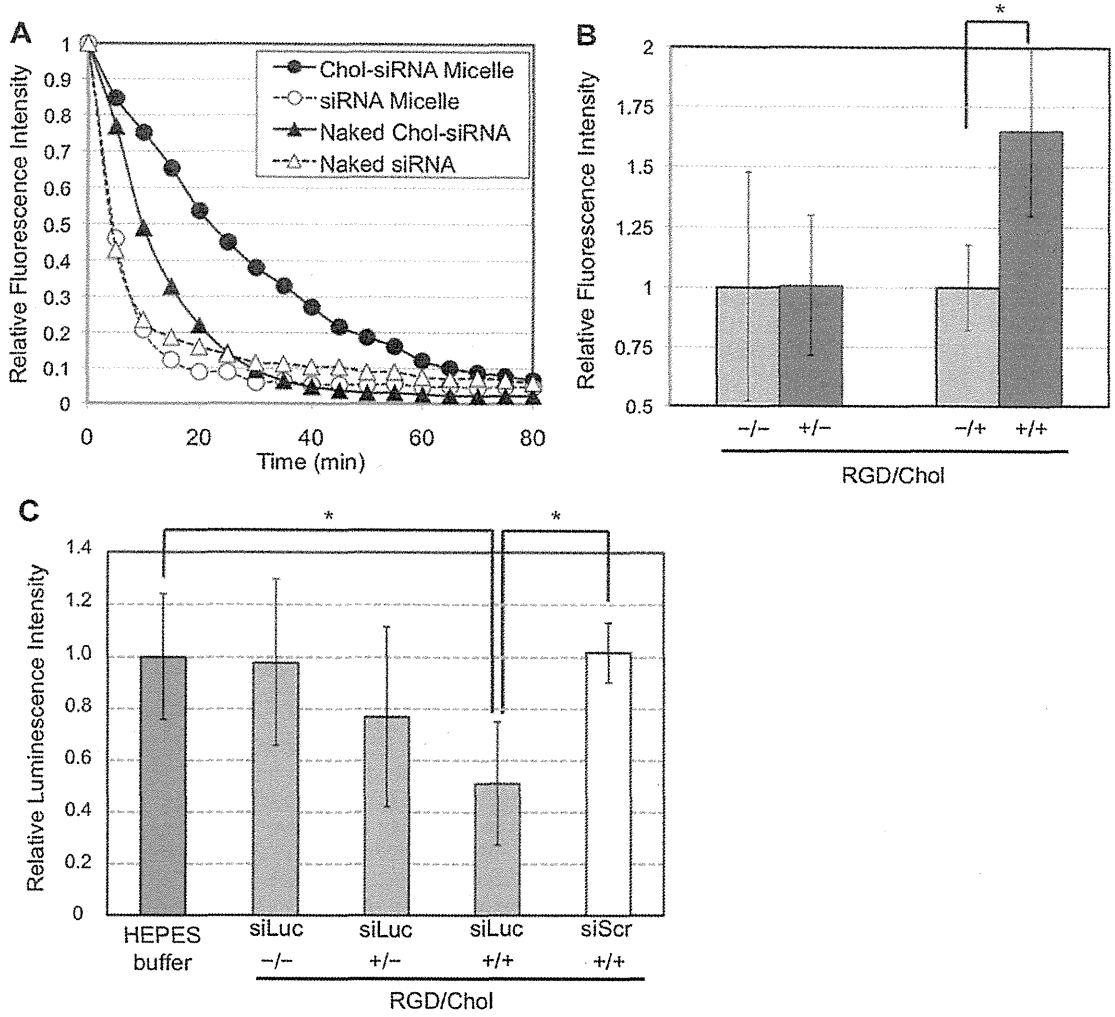


**Fig. 5.** *In vivo* performance of siRNA micelles. A) Blood circulation profiles, determined by IVRT-CLSM after intravenous injection (3.6 nmol siRNA/mouse) into BALB/c nude mice (open triangle: naked Chol-free/Cy5-siRNA, closed triangle: naked Chol/Cy5-siRNA, open circle: Chol-free/Cy5-siRNA micelles and closed circle: Chol/Cy5-siRNA micelles). Data represent the average value ($n = 3$). B) Relative accumulation of actively-targeted siRNA micelles to non-targeted controls in subcutaneous HeLa-Luc tumors (1.8 nmol siRNA/mouse) 4 h after intravenous injection into BALB/c nude mice. Fluorescence intensity from excised tumors was measured with an IVIS instrument, followed by the normalization as described in the Section 2.12. Data represent the average value ± standard deviation ($n = 4$ or 5, *: $p < 0.05$). C) Luciferase gene silencing activity of siRNA micelles in subcutaneous HeLa-Luc tumors. siRNA micelles were intravenously injected (1.8 nmol siRNA/mouse/injection) at 48, 38 and 24 h prior to measurement of the luminescence intensity from the excised tumors. The obtained luminescence intensity was normalized to that from the buffer-treated control tumors and the tumor volume. Data represent the average value ± standard deviation ($n = 5$, *: $p < 0.05$).

directed toward more uniform and stable micelle formation. Altogether, siRNA micelles prepared at +:− = 1.4 were used for subsequent experiments owing to the similarity in size between the two formulations as well as the sample homogeneity (lowest PDI). It should be further noted that the size distribution histograms were similar between non-targeted Chol-siRNA micelles prepared with PEG-PLL(MPA) and targeted Chol-siRNA micelles prepared with cRGD-PEG-PLL(MPA) at +:− = 1.4 (Fig. S4), suggesting that the cRGD peptide does not affect PIC formation with Chol-siRNA.

### 3.3. Stability of Chol-siRNA micelles

To confirm the stabilizing effect of cholesterol, the sizes of Chol-siRNA micelles and Chol-free micelles were determined under diluted conditions in 10% FBS-containing PBS by FCS measurement, which allows monitoring of the hydrodynamic size (or diffusion coefficient) of fluorescently labeled nanoparticles even in the presence of abundant serum proteins [16]. Indeed, this measurement determined the diffusion coefficients of Cy5-siRNA or Chol/Cy5-siRNA molecules complexed with the polymers, followed by conversion to hydrodynamic diameters based on the Stokes-Einstein equation (Fig. 3A). Whereas the original size of Chol-free micelles (ca. 40 nm) was maintained at 200 nM Cy5-siRNA, further dilution below 20 nM Cy5-siRNA dramatically decreased the micelle size, indicating disruption of Chol-free micelles upon dilution in the presence of FBS. It should be noted that the size of disrupted micelles (ca. 20 nm) was significantly larger than that of naked Cy5-siRNA (ca. 5 nm), suggesting that the micelles might be fragmented into small PIC fractions with a low association number of Cy5-siRNAs and block copolymers upon dilution, possibly due to limited intermolecular disulfide cross-linking within the micelle core. In contrast, Chol-siRNA micelles maintained their original size after dilution with 10% FBS, demonstrating the stabilizing effect of Chol moieties for maintaining micelle structure integrity.